OPEN ACCESS



Relative Intrinsic Scatter in Hierarchical Type Ia Supernova Sibling Analyses: Application to SNe 2021hpr, 1997bq, and 2008fv in NGC 3147

Sam M. Ward 1 , Stephen Thorp 1,2, Kaisey S. Mandel 1,3,4 , Suhail Dhawan 1 , David O. Jones 5 , Kirsty Taggart 5, Ryan J. Foley 5 , Gautham Narayan 6,7 , Kenneth C. Chambers 6 , David A. Coulter 5 , Kyle W. Davis 5 , Thomas de Boer 8 , Kaylee de Soto 9,10, Nicholas Earl 6, Alex Gagliano 6,7 , Hua Gao 8 , Jens Hjorth 11 , Mark E. Huber 8 , Luca Izzo 11 , Luca Izzo 11 , Armin Rest 12,13 , César Rojas-Bravo 5 , and Radosław Wojtak 11 (Young Supernova Experiment)

¹ Institute of Astronomy and Kavli Institute for Cosmology, Madingley Road, Cambridge, CB3 0HA, UK; smw92@cam.ac.uk
² The Oskar Klein Centre, Department of Physics, Stockholm University, AlbaNova University Centre, SE 106 91 Stockholm, Sweden
³ Statistical Laboratory, DPMMS, University of Cambridge, Wilberforce Road, Cambridge, CB3 0WB, UK
⁴ The Alan Turing Institute, Euston Road, London, NW1 2DB, UK
⁵ Department of Astronomy and Astrophysics, University of California, Santa Cruz, CA 95064, USA
⁶ University of Illinois at Urbana-Champaign, 1003 W. Green Street, IL 61801, USA
⁷ Centre for Astrophysical Surveys, National Centre for Supercomputing Applications, Urbana, IL 61801, USA
⁸ Institute for Astronomy, University of Hawaii, 2680 Woodlawn Drive, Honolulu, HI 96822, USA
⁹ Department of Astronomy & Astrophysics, The Pennsylvania State University, University Park, PA 16802, USA
¹⁰ Institute for Computational & Data Sciences, The Pennsylvania State University, University Park, PA 16802, USA
¹¹ DARK, Niels Bohr Institute, University of Copenhagen, Jagtvej 128, DK-2200 Copenhagen, Denmark
¹² Department of Physics and Astronomy, The Johns Hopkins University, Baltimore, MD 21218, USA
¹³ Space Telescope Science Institute, Baltimore, MD 21218, USA *Received 2023 February 24; revised 2023 August 31; accepted 2023 August 31; published 2023 October 13*

Abstract

We present Young Supernova Experiment grizy photometry of SN 2021hpr, the third Type Ia supernova sibling to explode in the Cepheid calibrator galaxy, NGC 3147. Siblings are useful for improving SN-host distance estimates and investigating their contributions toward the SN Ia intrinsic scatter (post-standardization residual scatter in distance estimates). We thus develop a principled Bayesian framework for analyzing SN Ia siblings. At its core is the cosmology-independent relative intrinsic scatter parameter, σ_{Rel} : the dispersion of siblings distance estimates relative to one another within a galaxy. It quantifies the contribution toward the total intrinsic scatter, σ_0 , from within-galaxy variations about the siblings' common properties. It also affects the combined distance uncertainty. We present analytic formulae for computing a σ_{Rel} posterior from individual siblings distances (estimated using any SN model). Applying a newly trained BAYESN model, we fit the light curves of each sibling in NGC 3147 individually, to yield consistent distance estimates. However, the wide σ_{Rel} posterior means $\sigma_{Rel} \approx \sigma_0$ is not ruled out. We thus combine the distances by marginalizing over σ_{Rel} with an informative prior: $\sigma_{Rel} \sim U(0, \sigma_0)$. Simultaneously fitting the trio's light curves improves constraints on distance and each sibling's individual dust parameters, compared to individual fits. Higher correlation also tightens dust parameter constraints. Therefore, σ_{Rel} marginalization yields robust estimates of siblings distances for cosmology, as well as dust parameters for siblinghost correlation studies. Incorporating NGC 3147's Cepheid distance yields $H_0 = 78.4 \pm 6.5 \,\mathrm{km \, s^{-1} \, Mpc^{-1}}$. Our work motivates analyses of homogeneous siblings samples, to constrain σ_{Rel} and its SN-model dependence.

Unified Astronomy Thesaurus concepts: Type Ia supernovae (1728); Distance indicators (394); Interstellar dust extinction (837); Astrostatistics (1882); Cosmology (343); Light curves (918)

Supporting material: machine-readable table

1. Introduction

Type Ia supernovae (SNe Ia) are standardizable candles, used to measure luminosity distances and constrain cosmological parameters (Riess et al. 1998, 2022; Perlmutter et al. 1999; Abbott et al. 2019; Freedman 2021; Stahl et al. 2021; Brout et al. 2022; Jones et al. 2022). The increasing number of observed SNe Ia (e.g., Riess et al. 1999; Jha et al. 2006; Hicken et al. 2009, 2012; Krisciunas et al. 2017; Foley et al. 2018; Hounsell et al. 2018; Abbott et al. 2019; Ivezić et al. 2019; Jones et al. 2021; Rose et al. 2021; Jones et al. 2022;

Original content from this work may be used under the terms of the Creative Commons Attribution 4.0 licence. Any further distribution of this work must maintain attribution to the author(s) and the title of the work, journal citation and DOI.

Scolnic et al. 2022; Brout et al. 2022) means cosmological analyses will be dominated by systematic uncertainties, rather than statistical uncertainties. Key to reducing these systematics is to understand the origin of the \approx 0.1 mag total intrinsic scatter, σ_0 , i.e., the post-standardization residual scatter in SN distance estimates compared to a best-fit cosmology (Scolnic et al. 2019; Brout & Scolnic 2021).

SN Ia siblings—SNe Ia that occur in the same host galaxy—are valuable for investigating standardization systematics (Elias et al. 1981; Hamuy et al. 1991; Stritzinger et al. 2011; Brown et al. 2015; Gall et al. 2018; Burns et al. 2020; Scolnic et al. 2020, 2022; Graham et al. 2022; Kelsey 2023). Siblings share common properties, like distance, redshift, and host galaxy stellar mass. Consequently, the relative dispersion of siblings distance estimates has no contribution from a variation of these

common properties. This mitigation of systematic uncertainties can yield insights into the origin of the total intrinsic scatter. Siblings are also useful for improving distance estimates to the host galaxy, by combining individual siblings distances.

In this work, we develop a principled Bayesian framework for robustly analyzing SN Ia siblings. We do this by introducing the "relative intrinsic scatter" parameter, $\sigma_{\rm Rel}$. This is the intrinsic scatter of individual siblings distance estimates relative to one another within a galaxy. It is constrained without assuming any cosmology, and it quantifies the contribution toward the total intrinsic scatter, σ_0 , from within-galaxy variations about the siblings' common properties.

We model $\sigma_{\rm Rel}$ to analyze a unique trio of SN Ia siblings in NGC 3147—the only Cepheid calibrator galaxy to host three SNe Ia. We advance on previous state-of-the-art single-galaxy siblings studies. Like Hoogendam et al. (2022) and Barna et al. (2023), we find strong consistency between individual siblings distance estimates, but we compute a σ_{Rel} posterior to assess the probability that $\sigma_{Rel} > 0$. Further, we marginalize over σ_{Rel} with an informative prior, $\sigma_{Rel} \sim U(0, \sigma_0)$, to robustly quantify the uncertainty on a combined distance estimate. For the first time, we simultaneously fit siblings light curves to yield improved constraints on distance and host galaxy dust parameters, compared to individual fits. Similarly to Biswas et al. (2022), we study the SN Ia color-luminosity relation in a cosmologyindependent fashion, but we constrain a physically motivated common host galaxy dust-law parameter R_V . Like Gallego-Cano et al. (2022), we use a single sibling's calibrator calibrator galaxy to estimate the Hubble constant. Our inference is dominated by the Cepheid distance measurement error; nonetheless, for the first time, we robustly propagate the siblings' combined uncertainty into a cosmological inference by marginalizing over σ_{Rel} .

We present our correlated intrinsic scatter model in Section 2. We then apply these concepts to fit NGC 3147's siblings. The data and model are described in Section 3 and Section 4, respectively; this includes new Pan-STARRS-1 *grizy* photometry of SN 2021hpr from the Young Supernova Experiment (Jones et al. 2021), as well as a new "W22" version of BAYESN (Mandel et al. 2022; Appendix A). We perform our analysis in Section 5 and conclude in Section 6.

2. Relative Intrinsic Scatter

2.1. Correlated Intrinsic Scatter Model

We decompose the distance estimate error terms originating from the total intrinsic scatter, $^{14} \delta M_s$, into common and relative components. The achromatic magnitude offset common to all siblings in a galaxy is $\delta M_{\rm Common}$, and the relative achromatic offsets—specific to each SN sibling—are $\delta M_{\rm Rel}$, where

$$\delta M_s = \delta M_{\text{Common}} + \delta M_{\text{Rel.s}}. \tag{1}$$

The population distributions of each component are

$$\delta M_{\text{Common}} \sim \mathcal{N}(0, \sigma_{\text{Common}}^2),$$

 $\delta M_{\text{Rel},s} \sim \mathcal{N}(0, \sigma_{\text{Rel}}^2).$ (2)

Their sum must have a dispersion equal to the total intrinsic scatter, σ_0 :

$$Var[\delta M_s] = \sigma_0^2 = \sigma_{Common}^2 + \sigma_{Rel}^2.$$
 (3)

The common intrinsic scatter, σ_{Common} , is thus the contribution toward σ_0 from population variations of the siblings' common properties. Meanwhile, the relative intrinsic scatter, σ_{Rel} , is the contribution toward σ_0 from within-galaxy variations about the siblings' common properties. This simple model can be applied in hierarchical Bayesian settings to robustly analyze siblings and combine individual siblings' distance estimates.

The uncertainty in a joint sibling distance estimate has a contribution, $Var[\overline{\delta M}]$, from the intrinsic scatter components:

$$\operatorname{Var}[\overline{\delta M}] = \sigma_0^2 - \sigma_{\operatorname{Rel}}^2 \left(1 - \frac{1}{N_{\operatorname{Siblings}}} \right), \tag{4}$$

where $\overline{\delta M}$ is the siblings' sample mean δM_s . Therefore, if the siblings are assumed to be perfectly correlated, $\sigma_{\rm Rel}=0$, the distance uncertainty contribution is σ_0 (it is maximized). But when the siblings are assumed to be perfectly uncorrelated, $\sigma_{\rm Rel}=\sigma_0$, the distance uncertainty contribution is minimized: $\sigma_0/\sqrt{N_{\rm Siblings}}$. Computing the precision-weighted average of individual siblings' distance estimates is equivalent to adopting this uncorrelated assumption, $\sigma_{\rm Rel}=\sigma_0$. Consequently, the joint distance uncertainty may be underestimated if in fact there is some correlation, i.e., $\sigma_{\rm Rel}<\sigma_0$.

2.2. σ_{Rel} Prior Knowledge

The size of the relative scatter is uncertain in the literature. On the one hand, Scolnic et al. (2020) and Scolnic et al. (2022) analyzed 8 and 12 sibling galaxies, respectively, using SALT2 (Guy et al. 2007, 2010), and their results indicated $\sigma_{\rm Rel}$ is large and comparable to the total intrinsic scatter, σ_0 . This implies the siblings' distance estimates are highly uncorrelated. On the other hand, Burns et al. (2020) constrain the dispersion of SNOOPY (Burns et al. 2011) distance differences between sibling pairs; after removing fast decliners, as well as SNe observed with the Neil Gehrels Swift Observatory, they use 11 sibling galaxies to estimate a 0.03 mag 95% upper bound on their dispersion hyperparameter. This is subdominant compared to the total intrinsic scatter in the Hubble diagram (typically $\sim 0.1-0.15$ mag), which implies the siblings' distance estimates are highly correlated. It is unclear then how σ_{Rel} compares to σ_0 and how this depends on the SN sample properties and the SN model used to estimate

A priori, we expect $\sigma_{\rm Rel} \leqslant \sigma_0$. This is because siblings in each galaxy share some common properties, which may otherwise vary in the population and directly contribute toward the total intrinsic scatter. These common properties include distance, redshift, peculiar velocity, and common host galaxy properties. The common host properties include both the global host galaxy properties, e.g., host galaxy stellar mass, and the siblings' mean local host galaxy properties, e.g., mean SFR, mean metallicity, mean stellar age, etc. The reported correlations of SN Ia Hubble residuals with global and/or local host galaxy properties (Sullivan et al. 2003, 2010; Kelly et al. 2010; D'Andrea et al. 2011; Childress et al. 2013; Rigault et al. 2013, 2020; Pan et al. 2014; Uddin et al. 2017; Jones et al. 2018; Roman et al. 2018; Rose et al. 2020; Smith et al. 2020;

¹⁴ The total δM_s parameter is the achromatic offset, with variance σ_0^2 , which contributes toward the total variance in the Hubble residuals, in addition to the redshift-based distance errors and the photometric distance measurement errors.

Uddin et al. 2020; Brout & Scolnic 2021; Johansson et al. 2021; Kelsey et al. 2021; Ponder et al. 2021; Popovic et al. 2021; Thorp et al. 2021; Briday et al. 2022; Meldorf et al. 2023; Thorp & Mandel 2022; Wiseman et al. 2022) indicates $\sigma_{\text{Common}} > 0$, or equivalently, $\sigma_{\text{Rel}} < \sigma_0$.

Moreover, σ_{Rel} is constrained without using "redshift-based distances," i.e., distances obtained by inputting estimates of cosmological redshift into a cosmological model. Therefore, σ_{Rel} has no error contribution from estimating cosmological redshift and assuming a cosmology; however, these two sources may contribute toward σ_0 if these additional errors—if any—are not already encompassed by the redshift-based distance uncertainties.

The contrast of σ_{Rel} versus σ_0 thus indicates whether it is within-galaxy variations or the population variation of the siblings' common properties that dominates σ_0 . We conclude that $0 \leqslant \sigma_{Rel} \leqslant \sigma_0$ is expected, and σ_{Rel} can be marginalized over with an informative flat prior:

$$\sigma_{\rm Rel} \sim U(0, \, \sigma_0).$$
 (5)

This is justified because the contributions toward σ_{Rel} are a subset of those that contribute toward σ_0 .

2.3. Constraining σ_{Rel}

We present analytic formulae for computing a σ_{Rel} posterior using individual siblings' distance estimates. In a single galaxy, we adopt a simple normal—normal hierarchical Bayesian model, as described in Chapter 5.4 of Gelman et al. (2013). Rewriting in our notation, we have $N_{\rm Siblings}$ individual distance estimates, $\hat{\mu}_s$, each with a measurement uncertainty, $\hat{\sigma}_{\rm fit,s}$, from fitting each set of siblings' light curves, \mathcal{D}_s . They are estimates of the distance plus the common and relative achromatic offsets, $\mu + \delta M_{\rm Common} + \delta M_{\rm Rel,s}$; therefore, there is a dispersion of the latent variables, which comes from the relative scatter: $\sigma_{\rm Rel}$. This is written as

$$\hat{\mu}_{s} \sim \mathcal{N}(\mu + \delta M_{\text{Common}}, \sigma_{\text{Rel}}^2 + \hat{\sigma}_{\text{fit.s}}^2).$$
 (6)

Using Equation (5.21) from Gelman et al. (2013) to marginalize over the distance and common offset, $\mu + \delta M_{\rm Common}$, and with a $\sigma_{\rm Rel}$ prior, $p(\sigma_{\rm Rel})$, we can compute an un-normalized relative scatter posterior:

$$p(\sigma_{\text{Rel}}|\mathcal{D}) \propto \frac{p(\sigma_{\text{Rel}}) \prod_{s=1}^{N_{\text{Siblings}}} \mathcal{N}(\hat{\mu}_s|\hat{\mu}_w, \hat{\sigma}_{\text{fit},s}^2 + \sigma_{\text{Rel}}^2)}{\sqrt{\sum_{s=1}^{N_{\text{Siblings}}} w_s}}, \quad (7)$$

$$w_s = \frac{1}{\hat{\sigma}_{\text{fit s}}^2 + \sigma_{\text{Rel}}^2} \; ; \quad \hat{\mu}_w = \frac{\sum_{s=1}^{N_{\text{Siblings}}} w_s \hat{\mu}_s}{\sum_{s=1}^{N_{\text{Siblings}}} w_s}, \tag{8}$$

where $\mathcal{D} = \{\mathcal{D}_s\}_{s=1}^{N_{\rm Siblings}}$. We note the single-galaxy $\sigma_{\rm Rel}$ likelihoods are conditionally independent (Bishop 2006). Therefore, a multigalaxy $\sigma_{\rm Rel}$ posterior is computed simply by multiplying the prior by the product of likelihoods in Equation (7). We use the siblings in NGC 3147 to compute a single-galaxy $\sigma_{\rm Rel}$ posterior in Section 5.1.

3. Data

We apply these concepts to analyze light curves of NGC 3147's trio of SN Ia siblings. We present new Young Supernova Experiment Pan-STARRS-1 *grizy* photometry of SN 2021hpr in Table 1 (Chambers et al. 2016). First detected on

2 April 2021 (Itagaki 2021), SN 2021hpr is the third spectroscopically confirmed normal Type Ia supernova in NGC 3147 (z = 0.00938), which is a high-stellar-mass Cepheid calibrator galaxy (Rahman et al. 2012; Yim & van der Hulst 2016; Sorai et al. 2019). The data were reduced with Photpipe (Rest et al. 2005), which has been used for numerous photometric reductions of YSE data (e.g., Kilpatrick et al. 2021; Tinyanont et al. 2022; Dimitriadis et al. 2022; Gagliano et al. 2022; Jacobson-Galán et al. 2022a, 2022b; Terreran et al. 2022). The YSE-PZ software was used for a transient discovery alert of SN 2021hpr, as well as for data collation, management, and visualization (Coulter et al. 2022, 2023). We present a spectrum of SN 2021hpr in Appendix B, which indicates it is a normal SN Ia. Recently, SN 2021hpr was studied using optical photometry and spectral observations (Zhang et al. 2022; Barna et al. 2023; Lim et al. 2023).

For the other two siblings, SNe 1997bq and 2008fv, we use the most up-to-date and well-calibrated Pantheon+¹⁵ light curves (Jha et al. 2006; Tsvetkov & Elenin 2010; Scolnic et al. 2022; summary in Table 2).

Figure 1 displays a Hubble Space Telescope image of NGC 3147, with the trio's locations marked. The image was constructed from stacked images produced by and retrieved from the Barbara A. Mikulski Archive for Space Telescopes (DOI:10.17909/k2kh-6h52), obtained from Programmes GO–15145 (PI Riess) and SNAP–16691 (PI Foley) between 2017 October 29th and December 2021 30th. The SN 2021hpr inset was created using the Trilogy software (Coe et al. 2012) using data from 2021 December 30th obtained through Programme SNAP–16691.

4. Modeling

We use BAYESN to fit each sibling's light curves individually, or all the siblings' light curves simultaneously. BAYESN is an optical-to-near-infrared hierarchical Bayesian model of the SN Ia SEDs (Thorp et al. 2021; Mandel et al. 2022). It uniquely enables us to fit the trio's optical-to-near-infrared light-curve data in order to coherently estimate distance and dust parameters.

4.1. New BAYESN Model: W22

The trio's data are in *BVRI* and *grizy* passbands, whereas previous iterations of BAYESN were trained either on *BVRIYJH* or *griz*, but not both. Therefore, we retrain a new and more robust BAYESN model (hereafter "W22") simultaneously on optical-NIR *BgVrizYJH* (0.35–1.8 μ m) data. The training sample combines the Foundation DR1 (Foley et al. 2018; Jones et al. 2019) and Avelino et al. (2019) samples, so it comprises 236 SNe Ia in host galaxies that are \approx 70% highmass (log₁₀(M_*/M_\odot) > 10). This sample does not include the siblings trio analyzed in this work. Population hyperparameters learned in W22 model training include the global dust-law shape, $R_V = 2.659$, and the total intrinsic scatter, $\sigma_0 = 0.094$ mag. Appendix A provides further details on this new model.

4.2. Fitting Procedures

To correct for Milky Way extinction, we use the Fitzpatrick (1999) law, adopting $R_{V:MW} = 3.1$, and a reddening estimate E

¹⁵ https://github.com/PantheonPlusSH0ES/DataRelease.git

Table 1New SN 2021hpr *grizy* Photometry, Observed with Pan-STARRS-1 as Part of the Young Supernova Experiment (Jones et al. 2021)^a

MJD	Phase ^b	g°	σ_g	r	σ_r	i	σ_i	z	σ_z	у	σ_y
59312.38	-8.99	15.055	0.006	15.109	0.005	15.499	0.007	15.464	0.008	15.567	0.015
59313.37	-8.01	14.889	0.004	14.913	0.004	15.283	0.004	15.332	0.005	15.409	0.012
59314.29	-7.10	14.710	0.003	14.785	0.003	15.123	0.004	15.223	0.005	15.297	0.009
59315.24	-6.16					15.013	0.004	15.092	0.005	15.230	0.009
59315.25	-6.15	14.592	0.004	14.659	0.003						

Notes.

^a The full table is available in machine-readable format in the online version of this article.

(This table is available in its entirety in machine-readable form.)

Table 2
Data Set Summary of NGC 3147's SN Ia Trio

SN Alias		Reference	Passbands	
2021hpr	21hpr	Table 1	grizy	
2008fv	08fv	Scolnic et al. (2022)	BVR	
1997bq	97bq	Scolnic et al. (2022)	BVRI	

Note

 $^{^{}m a}$ Only the passbands that can be fitted with BAYESN are shown, which excludes the SN 1997bq U-band data.

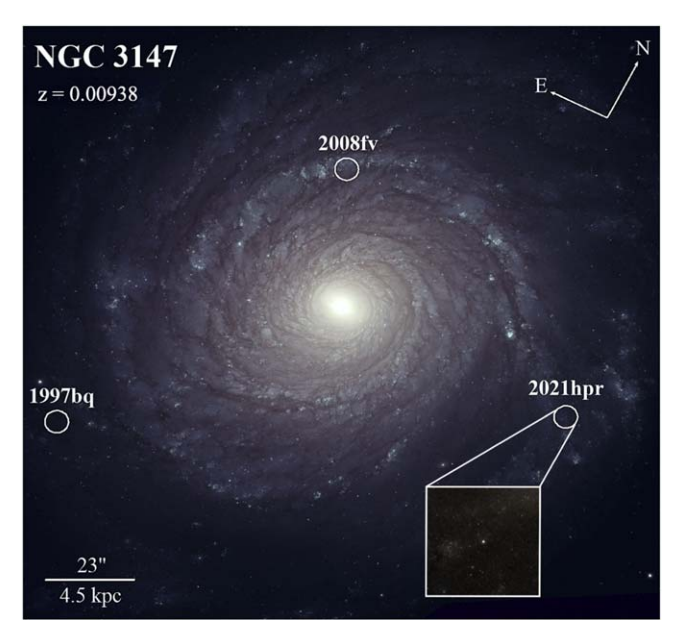


Figure 1. Hubble Space Telescope image of NGC 3147 ($z_{\rm Helio} = 0.00938$), with the SN Ia trio's locations marked and the length scale in the bottom left. Overlaid is a $15\rlap.{''}8 \times 15\rlap.{''}8$ (3 kpc on a side) inset region of SN 2021hpr from 2021 December 30th (≈ 9 months after SN detection).

 $(B-V)_{\rm MW}=0.024$ mag from Scolnic et al. (2022). To model host galaxy dust, we fit for each sibling's dust-law shape parameter, R_V^s , using a flat prior: $R_V^s \sim U(1, 6)$. The lower bound is based on the Rayleigh scattering limit $R_V \approx 1.2$ (Draine 2003), and the upper bound is motivated by observational results of lines of sight in the Milky Way (Fitzpatrick 1999; Schlafly et al. 2016).

 Table 3

 Intrinsic Scatter Modeling Assumptions for Hierarchically Analyzing Siblings

Assumption	$\sigma_{\rm Rel}$ Prior	μ Uncertainty ^a	
δM -Uncorrelated	$\sigma_{\mathrm{Rel}} = \sigma_0$	$\sigma_0/\sqrt{N_{\rm Siblings}}$	
δM -Mixed	$\sigma_{\rm Rel} \sim U(0, \sigma_0)$	$(\sigma_0/\sqrt{N_{\rm Siblings}}, \sigma_0)^{\rm b}$	
δM -Common	$\sigma_{\mathrm{Rel}} = 0$	σ_0	

Notes.

^a The contribution toward the joint sibling distance uncertainty originating from the total intrinsic scatter.

The time of *B*-band maximum brightness, $T_{B;\text{max}}$, which defines rest-frame phase via

$$t = \frac{T_{\text{MJD}} - T_{B;\text{max}}}{1 + \tau_{\text{Halio}}},\tag{9}$$

is fitted for in an individual fit and thereafter frozen at the posterior mean time. Data outside the model phase range, -10 < t < 40 days, and data with SNR < 3, are removed from the fit.

4.3. Joint Sibling Fit Modeling Assumptions

In the new joint fits, ¹⁶ we fit all light curves of siblings in a single galaxy simultaneously, while applying a common distance constraint; this yields a posterior on a single distance hyperparameter.

To jointly fit the siblings, we must make an assumption about their correlation. While the total intrinsic scatter is learned in BAYESN model training, $\sigma_0 = 0.094$ mag, the σ_{Rel} value is unknown. Therefore, we can fit under three δM modeling assumptions shown in Table 3. We can assume the siblings are perfectly uncorrelated, perfectly correlated, or fit for and marginalize over σ_{Rel} while imposing an informative prior: $\sigma_{Rel} \sim U(0, \sigma_0)$. Respectively, these are the δM -Uncorrelated, δM -Common, or δM -Mixed assumptions (Table 3). Our default assumption is to marginalize over σ_{Rel} .

b Phase is computed with $(T_{B;\text{max}}, z_{\text{Helio}}) = (59321.46 \text{ days}, 0.00938)$ using Equation (9).

^c All photometry in magnitudes.

^b Marginalizing over σ_{Rel} means a posterior on σ_{Rel} is computed, which weights the common distance uncertainty accordingly. The uncertainty contribution given some value of σ_{Rel} is shown in Equation (4).

¹⁶ https://github.com/bayesn/bayesn-public/tree/siblings/BayeSNmodel/stan_files

Table 4
Posterior Summaries of SN Parameters from Individual Fits and the Joint Common- μ Fit to the Siblings' Light Curves

Fit Type/Summary	Data Set(s)	Bands	μ (mag)	A_V^s (mag)	θ_s	R_V^{sa}	$\hat{\sigma}_{\mathrm{fit},s}(\mathrm{mag})^{\mathrm{b}}$
Individual	21hpr 97bq 08fv	grizy BVRI BVR	33.131 ± 0.119 33.127 ± 0.157 33.256 ± 0.219	0.266 ± 0.069 0.404 ± 0.132 0.441 ± 0.200	-0.566 ± 0.097 0.134 ± 0.194 -0.607 ± 0.176	2.801 ± 1.249 2.758 ± 1.210 < 3.112(4.927)	0.071 0.128 0.198
Common- μ	21hpr 97bq 08fv	grizy BVRI BVR	33.169 ± 0.107	0.244 ± 0.061 0.379 ± 0.082 0.537 ± 0.097	$-0.562 \pm 0.094 \\ 0.143 \pm 0.178 \\ -0.580 \pm 0.158$	$\begin{array}{c} 2.572 \pm 1.174 \\ 2.546 \pm 0.949 \\ 2.860 \pm 0.754 \end{array}$	

Notes.

5. Analysis

5.1. Individual Fits

We first fit each of NGC 3147's siblings individually with the new W22 BAYESN model. Figure 2 shows the SN 2021hpr fit posteriors of (μ , A_V , θ , R_V): the distance modulus, dust extinction, light-curve shape, and dust-law shape, respectively. Appendix B shows the SN 1997bq and SN 2008fv individual-fit posteriors.

Table 4 shows posterior summaries. The distance estimates are strongly consistent with one another, with a 0.060 mag sample standard deviation of distance point estimates (Figure 3). This consistency indicates the data are reliable and the model is robust. However, this does not directly evidence that $\sigma_{\rm Rel} < \sigma_0$.

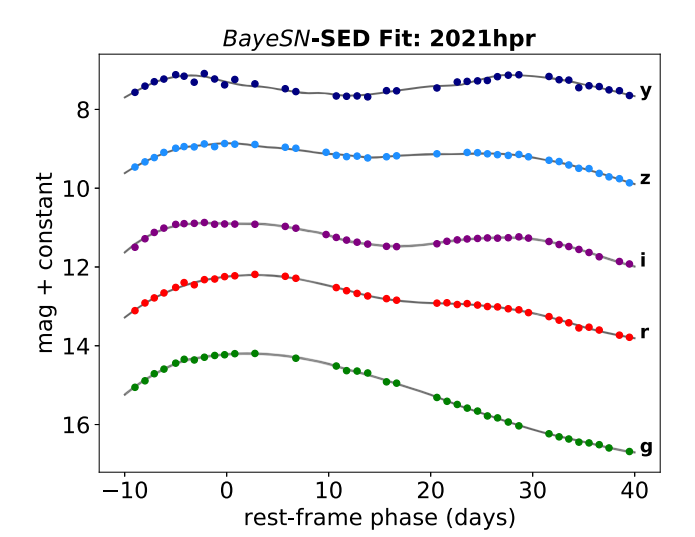
Instead, the important information is captured by the posterior on $\sigma_{\rm Rel}$. We compute cosmology-independent $\sigma_{\rm Rel}$ posteriors using the individual distance estimates, Equation (7), and Equation (8). We test the sensitivity to the choice of $\sigma_{\rm Rel}$ prior upper bound: (0.1, 0.15, 1) mag. To estimate distance measurement errors, or BAYESN "fitting uncertainties," $\hat{\sigma}_{\rm fit,s}$, we use

$$\hat{\sigma}_{\text{fit,s}} = \sqrt{\hat{\sigma}_{\mu,s}^2 - \hat{\sigma}_{0,s}^2},\tag{10}$$

where $(\hat{\sigma}_{\mu,s}, \hat{\sigma}_{0,s})$ are the posterior standard deviations of μ_s and δM_s , respectively.¹⁷

Figure 3 shows the $\sigma_{\rm Rel}$ posteriors. Although they peak at zero, the 68% (95%) posterior upper bounds are strongly prior dependent and extend out as far as $\sigma_{\rm Rel} < 0.21$ (0.67) mag. This shows, unsurprisingly, that the $\sigma_{\rm Rel}$ constraints are weak, and the trio's data alone do not rule out that $\sigma_{\rm Rel} > \sigma_0$. Therefore, the sample standard deviation of distance point estimates is a poor indicator of $\sigma_{\rm Rel}$. More sibling galaxies are required in order to tightly constrain $\sigma_{\rm Rel}$.

Nonetheless, we can robustly combine individual siblings' distances by marginalizing over $\sigma_{\rm Rel}$, while imposing an informative prior, $\sigma_{\rm Rel} \sim U(0, \, \sigma_0)$. To perform this marginalization, we build three simple models in the probabilistic programming language STAN (Carpenter et al. 2017; Stan Development Team 2020), corresponding to the three δM modeling assumptions in Table 3. We run each fit for 100,000 samples, which reduces the Monte Carlo error to <1 mmag.



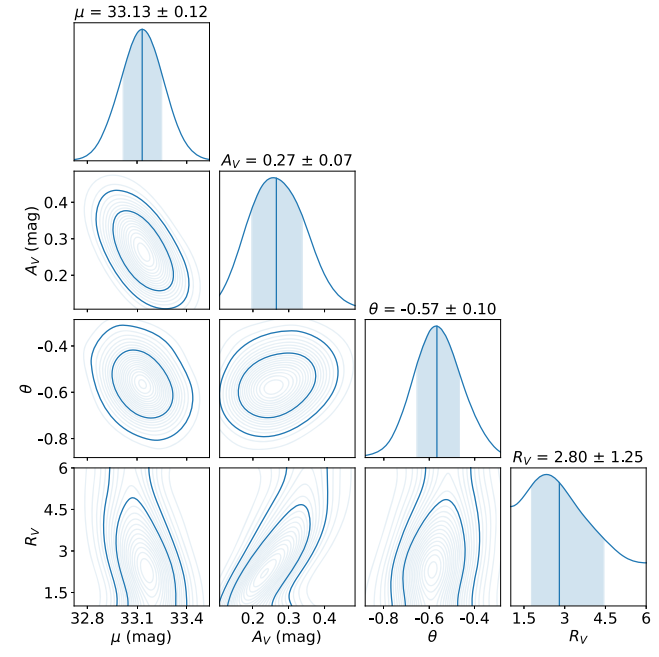


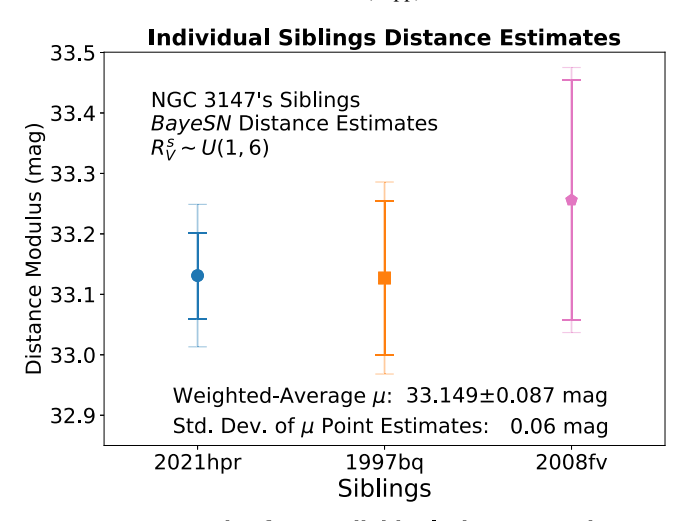
Figure 2. BAYESN fit to the SN 2021hpr *grizy* photometry (Table 1), along with kernel density estimates of the posterior distributions.

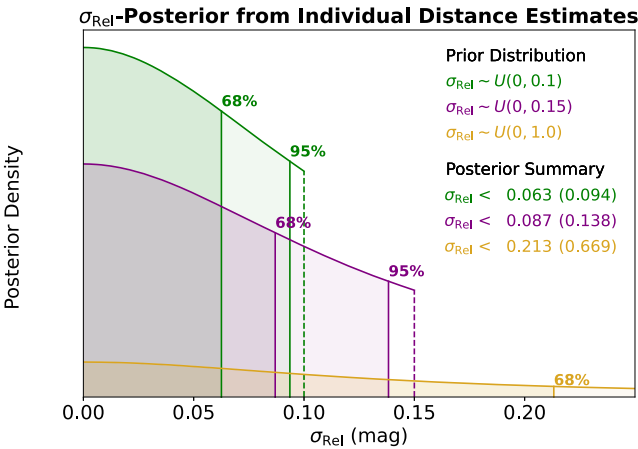
Results in Figure 3 show the distance uncertainty is minimized to a value of 0.087 mag when adopting the δM -Uncorrelated assumption. Meanwhile, marginalizing over $\sigma_{\rm Rel}$ returns a larger and more robust distance uncertainty:

^a The 68 (95)% quantiles are quoted for posterior peaking at zero. The dust-law shape priors are $R_V^s \sim U(1, 6)$.

b The fitting uncertainties, or "measurement errors," on the individual siblings distance estimates, computed using Equation (10).

¹⁷ The BAYESN fitting uncertainties are thus the contribution toward the individual distance uncertainties from fitting the time- and wavelength-dependent components.





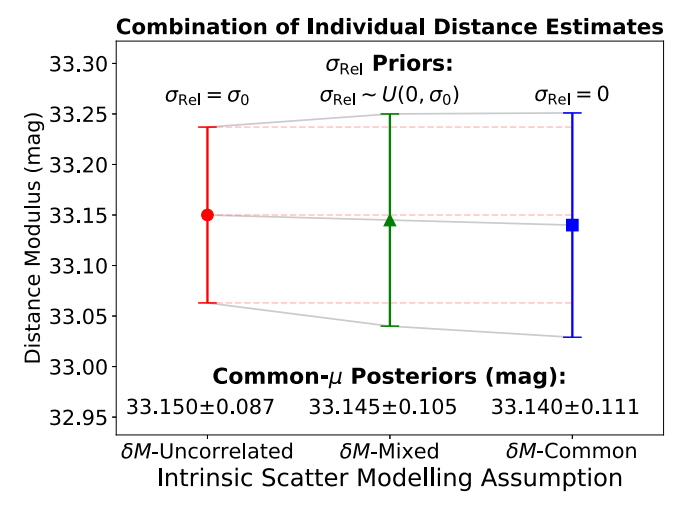


Figure 3. Analysis of individual siblings' distance estimates. (top) BAYESN distance estimates from individual fits to the sibling trio; error bars are the distance measurement errors [bold] and the total errors that include $\sigma_0=0.094$ mag [faint]. (middle) Posteriors of $\sigma_{\rm Rel}$ computed using analytic formulae in Section 2.3. Posteriors are weakly constraining, so more sibling galaxies are required in order to tightly constrain $\sigma_{\rm Rel}$. The 0.06 mag standard deviation is thus a poor estimator of $\sigma_{\rm Rel}$. (bottom) The individual distance estimates are combined under the three intrinsic scatter modeling assumptions (Table 3). The distance uncertainty is minimized when $\sigma_{\rm Rel}=\sigma_0$ is assumed, while the best estimate is obtained via $\sigma_{\rm Rel}$ marginalization.

0.105 mag. This methodology is inexpensive and can be implemented into cosmological analyses to improve joint sibling distance estimates.

5.2. BAYESN Joint Fits

Next, we apply the new BAYESN model architecture (Section 4.3) to jointly fit the siblings' light curves *simultaneously*, while imposing that the siblings have a common but unknown distance. Figure 4 displays the joint-fit posterior from marginalizing over $\sigma_{\rm Rel}$. As expected, the constraints on distance improve compared to individual fits (Table 4). Moreover, the constraints on each sibling's *individual* parameters are also improved by jointly fitting the siblings' light curves.

We visualize this in Figure 5, for SN 2008fv. This SN has optical *BVR* data only, and so it benefits greatly from the joint fit. In particular, the uncertainties in the individual dust parameters (A_V^s, R_V^s) reduce by $\approx (52, 29)\%$. Furthermore, the individual-fit R_V^s constraint peaks at the lower prior boundary $R_V^s = 1$, while the joint fit rules out low and unphysical values, to constrain $R_V^s = 2.86 \pm 0.75$.

The benefits of sibling data can be understood by drawing parallels with NIR data. Just as NIR data provide added leverage on the dust parameters, and hence the distance, so too do sibling data provide added leverage on the distance, which improves constraints on the remaining parameters, like the dust parameters.

To more precisely constrain R_V we assume it is the same for all three siblings. The common- R_V constraint from marginalizing over $\sigma_{\rm Rel}$ is $R_V = 2.62 \pm 0.67$. This is consistent with the W22 global value, $R_V = 2.659$, and the population mean, $R_V = 2.70 \pm 0.25$, constrained in Thorp et al. (2021). Figure 6 shows the increase in precision on R_V constraints, compared to individual fits.

We further fit under the other two intrinsic scatter modeling assumptions: δM -Uncorrelated and δM -Common. Figure 6 shows that the R_V uncertainties behave in the opposite sense to the distance uncertainty: with larger $\sigma_{\rm Rel}$ values, there is a larger dispersion of δM parameters and more freedom in the fit, which leads to larger R_V uncertainties. We check and assert that this trend also applies to all other chromatic parameters (like the dust extinction, A_V^s , and the light-curve shape parameters, θ_s). Therefore, like the distance, the best chromatic parameter constraints are obtained by marginalizing over $\sigma_{\rm Rel}$.

5.3. H₀ Constraints

Our work culminates in an estimate of the Hubble constant, obtained by simultaneously fitting the siblings trio's light curves, a Cepheid distance to NGC 3147 (Riess et al. 2022), and BAYESN distance estimates to 109 Hubble flow SNe Ia. This inference is motivated by the conclusion in Scolnic et al. (2020), which states: "Understanding the limited correlation between SNe in the same host galaxy will be important for SH0ES to properly propagate the combined uncertainty." While understanding the root cause of correlated intrinsic scatter is beyond the scope of this work, our new relative scatter model marginalizes over this correlation, leading to robust uncertainties. Moreover, correlated intrinsic scatter was neglected in the recent siblings- H_0 estimate in Gallego-Cano et al. (2022). This subsection thus demonstrates how siblings can be robustly modeled to estimate cosmological parameters.

We simultaneously fit the siblings' light curves with the Cepheid and Hubble flow distances, and we marginalize over $\sigma_{\rm Rel}$ using the informative prior: $\sigma_{\rm Rel} \sim U(0,\,\sigma_0)$. This extracts the most information out of the data via jointly fitting the siblings light curves, while accurately quantifying the distance

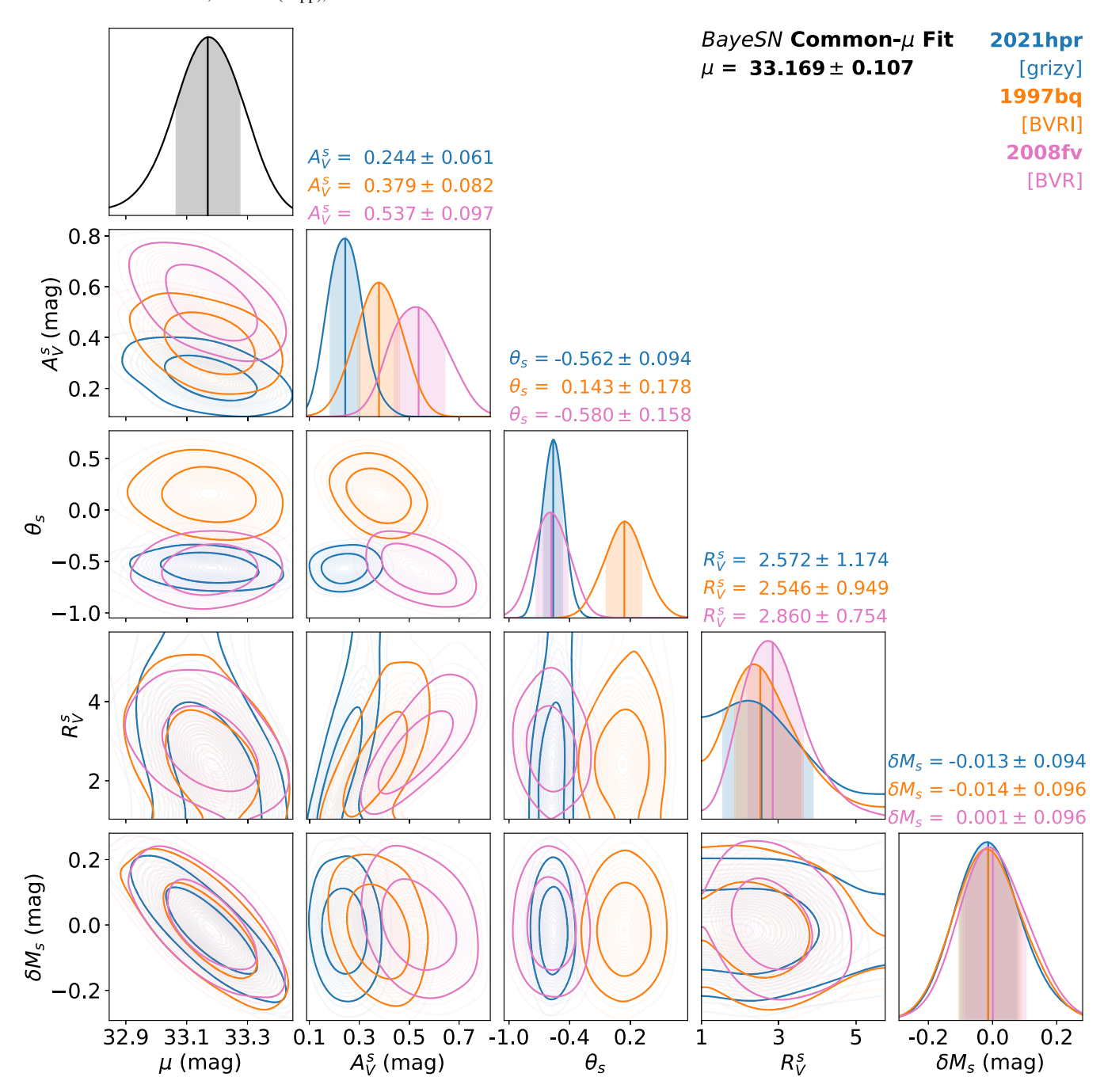


Figure 4. Posterior from the joint fit to NGC 3147's siblings' light curves. Constraints on the distance hyperparameter [black] and each sibling's individual parameters [colors] improve compared to individual fits. This fit marginalizes over σ_{Rel} with an informative prior, $\sigma_{Rel} \sim U(0, \sigma_0)$, and $\sigma_0 = 0.094$ mag, to yield robust estimates of the distance and chromatic parameters.

uncertainty via σ_{Rel} marginalization. Appendix C details our H_0 -inference methodologies further.

We estimate $H_0 = 78.4 \pm 6.5 \, \mathrm{km \, s^{-1} \, Mpc^{-1}}$. The posterior is displayed in Figure 7. In Appendix C, we show this result is insensitive to the siblings' R_V^s modeling assumptions, as well as their intrinsic scatter modeling assumptions. Assuming the siblings are uncorrelated yields $H_0 = 78.4 \pm 6.2 \, \mathrm{km \, s^{-1} \, Mpc^{-1}}$, meaning $\approx 1.7 \, \mathrm{km \, s^{-1} \, Mpc^{-1}}$ is added in quadrature to the H_0 uncertainty as result of marginalizing over σ_{Rel} . Equivalently, this is a $\approx 2.2\%$ increase in the H_0 uncertainty.

Our Hubble constant estimate is consistent with typical local Universe measurements, in particular $H_0 = 73.04 \pm 1.04 \,\mathrm{km \, s^{-1} \, Mpc^{-1}}$ (Riess et al. 2022), and also the lower *Planck* value: $H_0 = 67.4 \pm 0.5 \,\mathrm{km \, s^{-1} \, Mpc^{-1}}$ (Planck Collaboration et al. 2020). The statistical error dominates, and including more calibrator galaxies will lead to a more accurate and precise H_0 inference that is less sensitive to Cepheid modeling choices (as shown in Figure 18 in Riess et al. 2022; see also the companion paper by Dhawan et al. 2023). The siblings' correlation is a subdominant effect in this case study; nonetheless, we have demonstrated, for the first time, how to

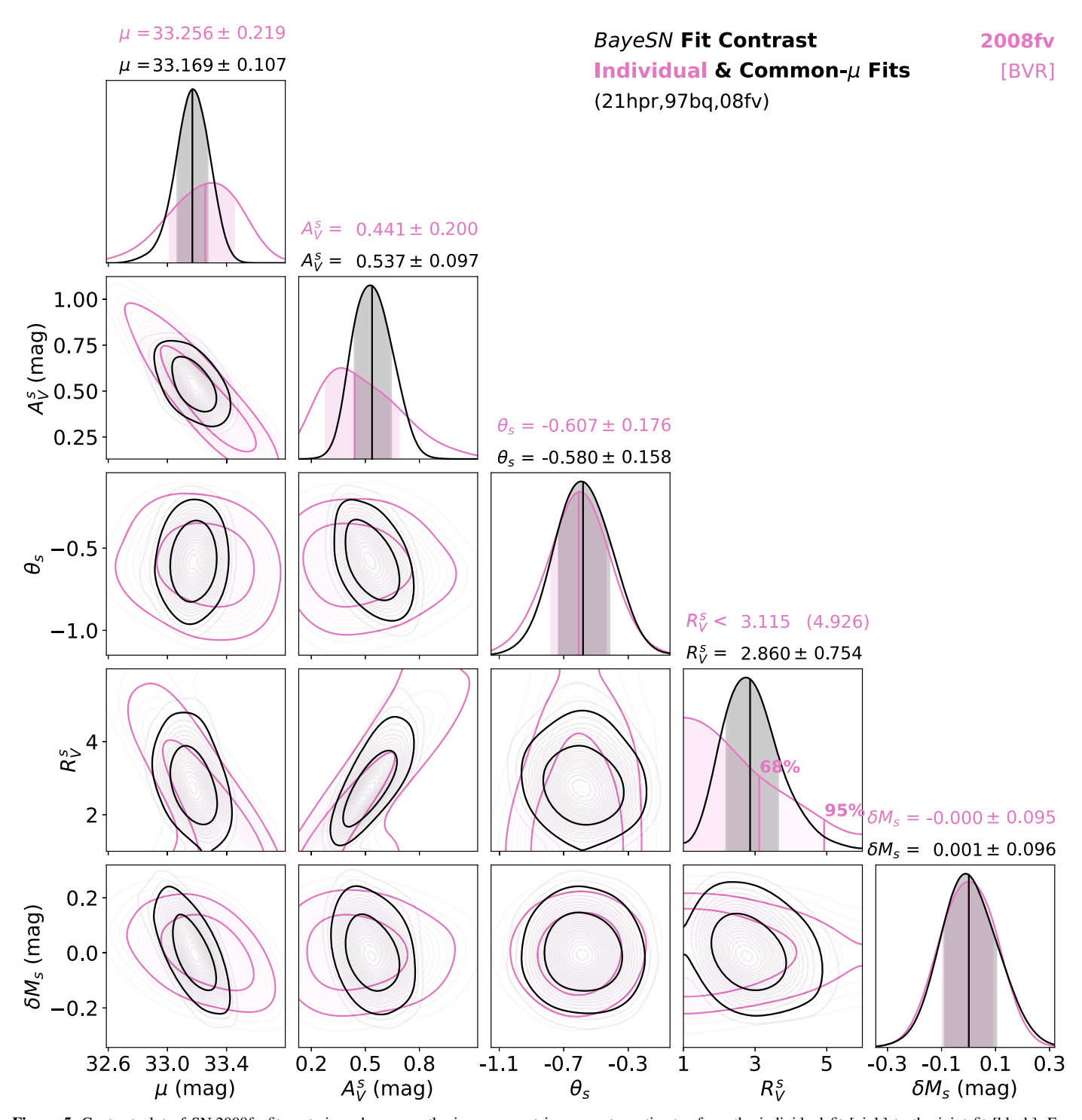


Figure 5. Contrast plot of SN 2008fv fit posteriors showcases the improvement in parameter estimates from the individual fit [pink] to the joint fit [black]. For example, the uncertainties on the individual dust parameters, (A_V^s, R_V^s) , shrink by $\approx (52, 29)\%$. With only *BVR* data in the individual fit, R_V^s constraints are weak; however, the joint fit rules out low unphysical values $R_V^s \approx 1$.

robustly propagate the siblings' combined uncertainty to infer cosmological parameters.

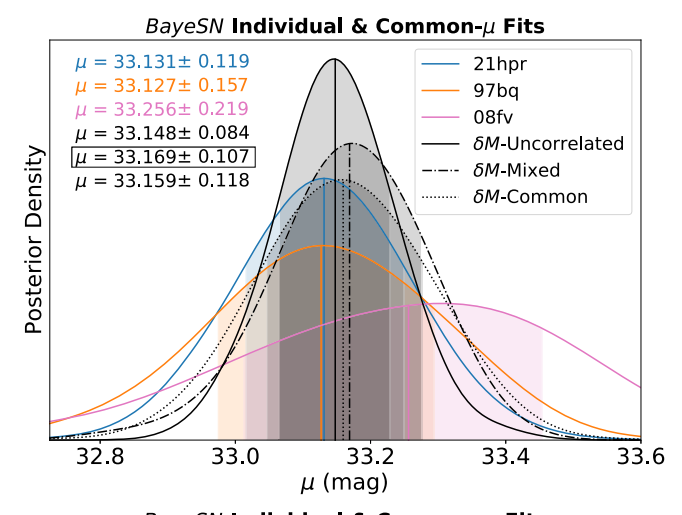
6. Conclusions

We have analyzed light curves of the SN Ia trio of siblings in the high-stellar-mass Cepheid calibrator galaxy NGC 3147. This includes PS1 *grizy* photometry of SN 2021hpr from the Young Supernova Experiment (Jones et al. 2021), presented in Table 1. We use a new publicly available W22 version of

the BAYESN hierarchical optical-to-near-infrared SN Ia SED model (Section 4.1, Appendix A), which we have retrained simultaneously on BgVrizYJH (0.35–1.8 μ m) data of 236 SNe Ia.

We summarize the key conclusions from this work:

1. The relative intrinsic scatter, σ_{Rel} , is the intrinsic scatter of individual siblings distance estimates relative to another within a galaxy. It quantifies the contribution



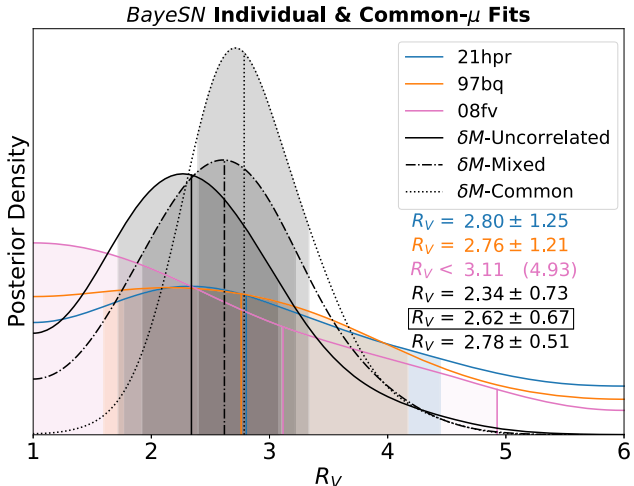


Figure 6. Chromatic parameter uncertainties are affected in the opposite sense to the distance hyperparameter by different intrinsic scatter modeling assumptions (Table 3). The overlay shows distance and common- R_V posteriors from individual fits [colors] and joint fits [black]. (top panel) Assuming the siblings are uncorrelated minimizes the distance estimate uncertainty, while marginalizing over σ_{Rel} yields robust uncertainties. (bottom panel) The common- R_V posteriors [black] show that the more correlated the intrinsic scatter components are, the less freedom there is in the fit, which results in tighter constraints on chromatic parameters. This is opposite to the behavior of the distance hyperparameter. Marginalizing over σ_{Rel} yields $R_V = 2.62 \pm 0.67$.

toward the total intrinsic scatter, σ_0 , from within-galaxy variations about the siblings' common properties, and it is constrained without assuming any cosmology. Therefore, it is distinct from σ_0 , and we expect $\sigma_{Rel} \leq \sigma_0$.

- 2. We present analytic formulae for computing a σ_{Rel} posterior from individual siblings distance estimates (Section 2.3). Applying this to NGC 3147's siblings, the posterior is wide, meaning the sample standard deviation of distance point estimates is a poor indicator of σ_{Rel} , in particular in this small sample size limit.
- 3. Assuming $\sigma_{\rm Rel} = \sigma_0$ will underestimate the uncertainty on a joint sibling distance estimate if in fact $\sigma_{\rm Rel} < \sigma_0$. An inexpensive way of constraining μ from individual siblings' distance estimates is to marginalize over $\sigma_{\rm Rel}$ with an informative prior: $\sigma_{\rm Rel} \sim U(0, \, \sigma_0)$.
- 4. For the first time, we hierarchically fit siblings' light curves simultaneously, to estimate a common, but unknown, distance hyperparameter. The BAYESN joint fit benefits from a hierarchical sharing of information,

- returning improved constraints on the common distance, as well as each sibling's *individual* chromatic parameters (e.g., light-curve shape and host galaxy dust parameters). For example, SN 2008fv's individual-fit R_V^s constraint peaks at $R_V^s = 1$, but the joint fit naturally rules out low unphysical values to constrain $R_V^s = 2.86 \pm 0.75$.
- 5. Chromatic parameters are also affected by $\sigma_{\rm Rel}$, and in the opposite sense to the distance, with larger $\sigma_{\rm Rel}$ values returning *larger* chromatic parameter uncertainties. Therefore, $\sigma_{\rm Rel}$ marginalization yields robust estimates of chromatic parameters, as well as the distance. We infer a common dust hyperparameter $R_V = 2.62 \pm 0.67$.
- 6. We estimate the Hubble constant, $H_0 = 78.4 \pm 6.5 \, \mathrm{km \, s^{-1} \, Mpc^{-1}}$, by hierarchically fitting the siblings' light curves with a Cepheid distance and Hubble flow distances, while marginalizing over $(\sigma_{\mathrm{Rel}}, A_V^s, R_V^s)$ in the calibrator galaxy and $(\sigma_0, \sigma_{\mathrm{pec}})$ in the Hubble flow. Marginalizing over σ_{Rel} adds $\approx 1.7 \, \mathrm{km \, s^{-1} \, Mpc^{-1}}$, or $\approx 2.2\%$, in quadrature to the H_0 uncertainty, compared to assuming $\sigma_{\mathrm{Rel}} = \sigma_0$. This inference is the first cosmological analysis to robustly propagate the combined uncertainty from SN Ia siblings.

This work provides a robust and principled Bayesian framework for hierarchically analyzing SN Ia siblings. Consequently, we have shown the relative intrinsic scatter, σ_{Rel} , is a key parameter in any sibling analysis. Marginalizing over σ_{Rel} yields robust inferences of siblings' distances for cosmology, and chromatic parameters for SN–host correlation studies. With more sibling galaxies, there is the potential to tightly constrain σ_{Rel} and compare it against σ_0 , in order to investigate the dominant systematics acting in BAYESN and other SN Ia models.

A multigalaxy $\sigma_{\rm Rel}$ inference may be sensitive to cross-calibration systematics originating from siblings observed on different photometric systems. While extensive work has gone into building distance covariance matrices for SALT2 distances in the Pantheon+ sample (Scolnic et al. 2022; Brout et al. 2022), building analogous covariance matrices for BAYESN is beyond the scope of this work. A workaround will be to analyze a sample of SN Ia siblings observed on a single photometric system, thus mitigating cross-calibration systematics. The near-future sample of ZTF DR2 siblings (Dhawan et al. 2022; Graham et al. 2022) is expected to contain ≈ 30 SN Ia sibling galaxies, so it will be an interesting test set for investigating $\sigma_{\rm Rel}$, and its SN-model dependence.

Beyond constraining σ_{Rel} , siblings are useful for studying within-galaxy dispersions of other features, like (A_V^s, θ_s, R_V^s) , and host properties (Scolnic et al. 2020, 2022; Biswas et al. 2022). Identifying and studying features that have within-galaxy dispersions that are smaller than their total dispersions may help to explain any correlations among siblings distance estimates.

Intermediate-sized samples of SN Ia siblings have already been compiled, numbering ~ 10 –40 siblings (e.g., Burns et al. 2020; Scolnic et al. 2020, 2022; Graham et al. 2022). The largest sibling sample to date was recently presented in Kelsey (2023), and it comprises 158 galaxies with 327 SNe Ia. The potential for discovering more siblings is promising, with surveys such as the Dark Energy Survey (DES; Scolnic et al. 2020; Smith et al. 2020), the Legacy Survey of Space and Time (LSST; The LSST Dark Energy Science Collaboration et al. 2018; Ivezić et al. 2019; Scolnic et al. 2020), the Nancy Grace

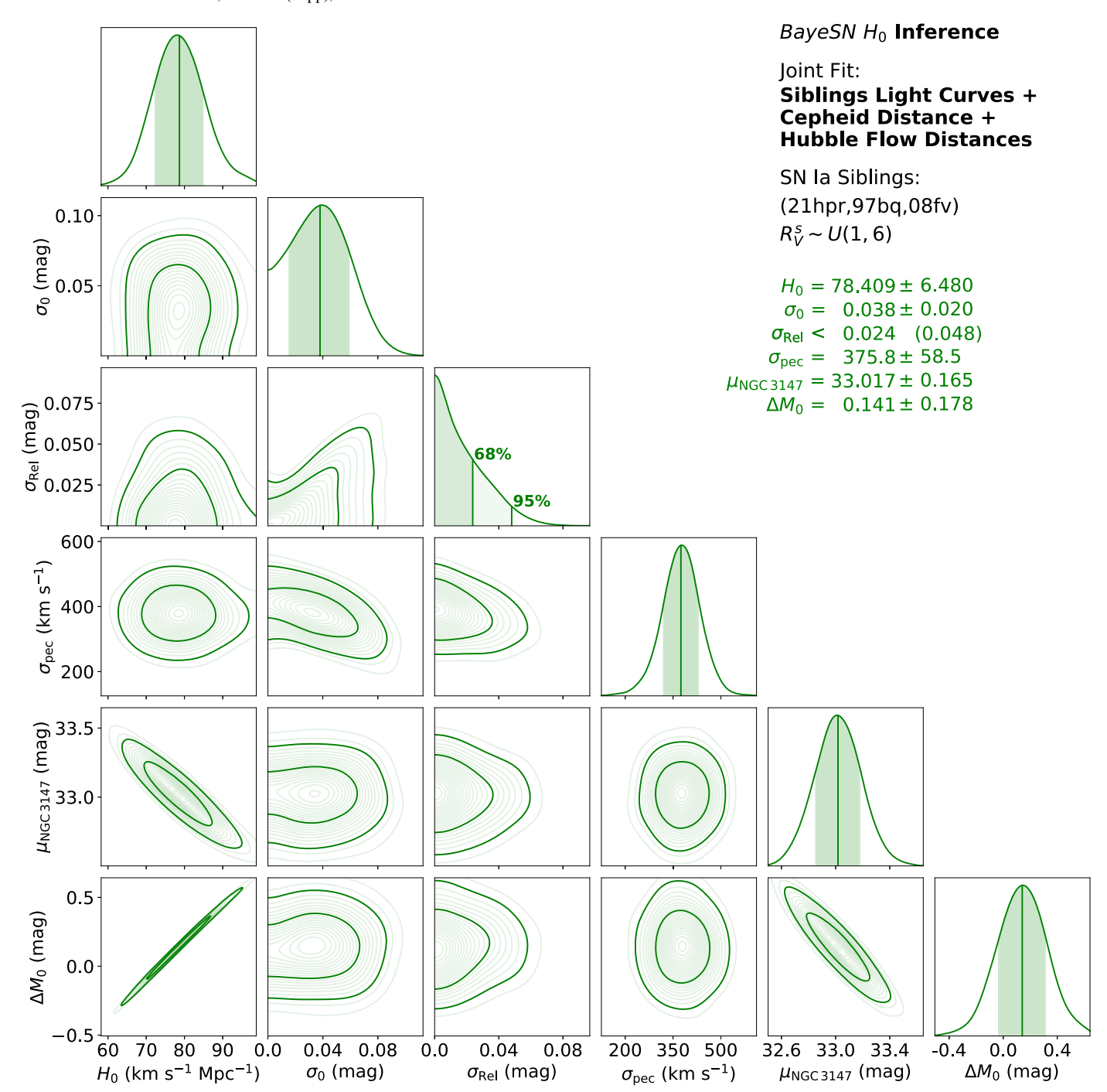


Figure 7. Hubble constant inference from simultaneously fitting NGC 3147's siblings' light curves, the Cepheid distance from Riess et al. (2022), and BAYESN distance estimates to 109 SNe Ia in the Hubble flow. We marginalize over the total intrinsic scatter, σ_0 , the siblings' relative intrinsic scatter, σ_{Rel} , and the peculiar velocity dispersion, σ_{pec} . Marginalizing over σ_{Rel} while jointly fitting the siblings' light curves yields the best NGC 3147 distance constraint. We estimate $H_0 = 78.4 \pm 6.5 \text{ km s}^{-1} \text{ Mpc}^{-1}$.

Roman Space Telescope (*Roman*; Hounsell et al. 2018; Rose et al. 2021), the Young Supernova Experiment (YSE; Jones et al. 2021), and the Zwicky Transient Facility (ZTF; Dhawan et al. 2022; Graham et al. 2022). Therefore, SN Ia siblings will be increasingly valuable for studying SN Ia standardization systematics in cosmological analyses in the years ahead.

Acknowledgments

We thank Adam G. Riess for providing the Cepheid distance to NGC 3147 prior to its public release on 18 July 2022.

S.M.W. was supported by the UK Science and Technology Facilities Council (STFC). S.T. was supported by the Cambridge Centre for Doctoral Training in Data-Intensive Science funded by STFC. K.S.M. acknowledges funding from the European Research Council under the European Unions Horizon 2020 research and innovation program (ERC grant Agreement No. 101002652). This project has also been made possible through the ASTROSTAT-II collaboration, enabled by the Horizon 2020, EU grant Agreement No. 873089. S.D. acknowledges support from the Marie Curie Individual Fellowship under grant ID 890695 and a Junior Research Fellowship at Lucy Cavendish College. D.O.J.

acknowledges support by NASA through the NASA Hubble Fellowship grant HF2-51462.001 awarded by the Space Telescope Science Institute, which is operated by the Association of Universities for Research in Astronomy, Inc., for NASA, under contract NAS5-26555. The UCSC team is supported in part by NASA grant NNG17PX03C, NSF grant AST-1815935, the Gordon & Betty Moore Foundation, the Heising-Simons Foundation, and by a fellowship from the David and Lucile Packard Foundation to R.J.F. G.N. was supported by the University of Illinois at Urbana-Champaign and the Center for Astrophysical Surveys at the National Center for Supercomputing Applications. Pan-STARRS is a project of the Institute for Astronomy of the University of Hawaii, and is supported by the NASA SSO Near Earth Observation Program under grants 80NSSC18K0971, NNX14AM74G, NNX12AR65G, NNX13AQ47G, NNX08AR22G, and by the State of Hawaii. K.D. acknowledges support in part by the NSF through grant AST-2108676. N.E. acknowledges funding from the Center for Astrophysical Surveys Fellowship through the National Center for Supercomputing Applications at the University of Illinois at Urbana-Champaign. A.G. is supported by the National Science Foundation Graduate Research Fellowship Program under grant No. DGE1746047. A.G. further acknowledges funding from the Center for Astrophysical Surveys Fellowship at UIUC/NCSA and the Illinois Distinguished Fellowship. This work was supported by a VILLUM FONDEN Investigator grant (project number 16599 and 25501). This work made use of the Illinois Campus Cluster, a computing resource that is operated by the Illinois Campus Cluster Program (ICCP) in conjunction with the National Center for Supercomputing Applications (NCSA) and is supported by funds from the University of Illinois at Urbana-Champaign.

Facilities: Pan-STARRS-1, HST.

Appendix A W22 BAYESN Model

Here, we describe the training and performance of the new W22 version of BAYESN. ¹⁸ The W22 training sample combines the T21 and M20 training samples. The M20 training sample comprises 79 SNe Ia from Avelino et al. (2019), observed in *BVRIYJH* passbands, compiled across a range of telescopes and surveys (Jha et al. 1999; Krisciunas et al. 2003, 2004a, 2004b, 2007; Stanishev et al. 2007; Pignata et al. 2008; Wood-Vasey et al. 2008; Hicken et al. 2009, 2012; Leloudas et al. 2009; Friedman et al. 2015; Krisciunas et al. 2017). This sample is approximately 80% high-mass ($\log_{10}(M_*/M_\odot) > 10$). The T21 training sample comprises 157 SNe Ia from the untargeted Foundation DR1 survey, observed in *griz* passbands with the Pan-STARRS-1 system (Foley et al. 2018; Jones et al. 2019). This sample has a 48:109 split at $\log_{10}(M_*/M_\odot) \approx 10$ and a median mass at $\log_{10}(M_*/M_\odot) \approx 10.331$.

The training procedure and all hyperpriors are exactly as described in Mandel et al. (2022), with the exception of the priors on the intrinsic residual standard deviation vector, σ_{ϵ} . Where Mandel et al. (2022) used an uninformative half-Cauchy prior with unit scale on each element of this vector, here we place an uninformative half-normal prior with a scale of 0.15, i.e., $P(\sigma_{\epsilon,q}) = \text{Half} - \mathcal{N}(\sigma_{\epsilon,q}|\mu = 0, \sigma = 0.15)$ for the qth

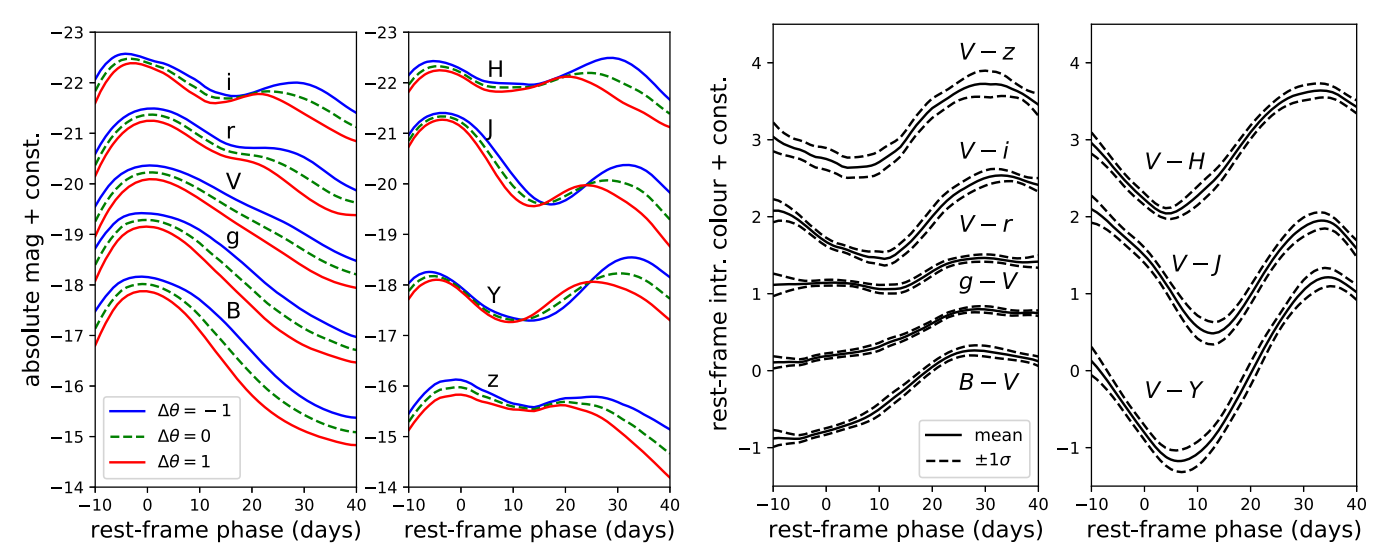


Figure 8. (Left panel) Rest-frame light curves in BgVrizYJH passbands are synthesized using the new W22 BAYESN model, to illustrate the intrinsic effect of $W_1(t,\lambda)$, the first functional principal component (FPC). Dust extinction and residual functions are set to zero, and the coefficient on the first FPC, θ , is varied about the population mean; this variation gives rise to the Phillips (1993) "broader-brighter" empirical relation in optical passbands, while also affecting the NIR amplitudes and times of the second peak. For visual clarity, the BgVrizYJH light curves have been vertically offset by (1.25, 0, -1, -2.25, -4, 2.5, 0.25, -2.75, -4) mag, respectively. (right panel) Rest-frame intrinsic color curves are synthesized using the new W22 BAYESN model, to illustrate the predicted level of residual intrinsic color variation after correction for dust extinction and light-curve shape. Dust extinction and the light-curve shape, θ , are set to zero. The solid black lines depict the mean intrinsic color curves, while the dashed lines show a 1 σ variation about the mean, computed by taking the standard deviation of many residual function realizations, each drawn from the intrinsic SED residual covariance matrix. For visual clarity, the colors are offset by (-0.75, 0.25, 1.25, 2.5, 3.5, 0.25, 2.25, 3.25) mag for (B - V, g - V, V - r, V - i, V - z, V - Y, V - J, V - H), respectively.

¹⁸ https://github.com/bayesn/bayesn-model-files

element. This provides better regularization in the z-band and NIR, and it can be interpreted as assuming that the residual scatter in any band at any given time is <0.3 mag with 95% prior probability.

We verify the robustness of the W22 model by computing the RMS and σ_{-pv} values in the Hubble diagram, from fits to the full sample of 236 SNe Ia¹⁹. The (RMS, σ_{-pv}) values are (0.129, 0.113) mag. From W22 fits to each of the T21 and M20 samples, the values are (0.129, 0.117) mag and (0.130, 0.104) mag, respectively. This compares well to the Hubble diagram statistics obtained from fitting T21, (0.124, 0.112) mag, and M20, (0.137, 0.109) mag, to their respective training samples. When fitting W22 to the 40 SN Ia "NIR@max" subsample from Mandel et al. (2022), the fit statistics are (0.093, 0.085) mag, as compared to the M20 values: (0.096, 0.083) mag.

The effect of the first functional principal component (FPC) is showcased in the left panels of Figure 8, and the population variations in intrinsic color are showcased in the right panels of Figure 8. The posterior means of the population hyperparameters learned in W22 model training (in addition to the FPCs and residual covariance matrix) are the global dust-law shape, $R_V = 2.659$, the dust extinction hyperparameter, $\tau_A = 0.252$ mag, and the total intrinsic scatter, $\sigma_0 = 0.094$ mag.

Appendix B **Additional Sibling Data and Fits**

The SN 2021hpr spectrum in Figure 9 was obtained with the Kast spectrograph on the Lick Shane telescope (Miller & Stone 1993) on 2021 April 13th, \approx 4.2 days before *B*-band maximum brightness. The data were reduced with standard CCD processing and extractions using a custom data reduction pipeline.²⁰ which

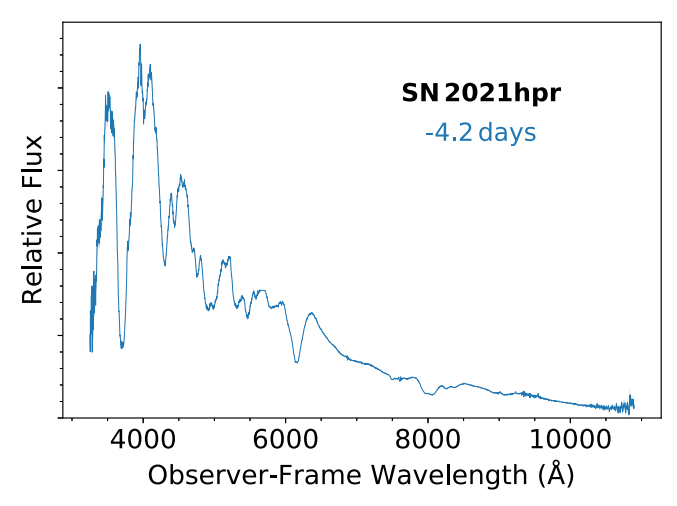


Figure 9. Spectrum of SN 2021hpr, observed \approx 4.2 days before the *B*-band maximum, using the Kast spectrograph on the Lick Shane telescope, in the observer-frame wavelength range: 3254-10894 Å.

employs IRAF.²¹ We fit low-order polynomials to calibrationlamp spectra and perform small shifts based on sky lines in object frames to determine a wavelength solution. We employ custom Python routines and spectrophotometric standard stars to flux calibrate the spectrum and remove telluric lines (Silverman et al. 2012). We remove data and linearly interpolate the spectrum between 5650 Å and 5710 Å in the observer frame so as to remove a ghosting artifact.

Figure 10 shows individual BAYESN fits to the Pantheon + (Scolnic et al. 2022) light curves of SNe 1997bq and 2008fv. Table 5 records posterior summaries from fixed- R_V individual fits to the trio ($R_V^* = 2.659$).

 $[\]overline{^{19}}$ The $\sigma_{-\mathrm{pv}}$ statistic is an estimate of the dispersion in the Hubble residuals, removing the expected contribution from peculiar velocity uncertainties (as defined in Equation (32) of Mandel et al. (2022) and adopting $\sigma_{\rm pec} = 150 \ {\rm km \ s^{-1}}$). https://github.com/msiebert1/UCSC_spectral_pipeline

²¹ IRAF was distributed by the National Optical Astronomy Observatory, which was managed by the Association of Universities for Research in Astronomy (AURA) under a cooperative agreement with the National Science Foundation.

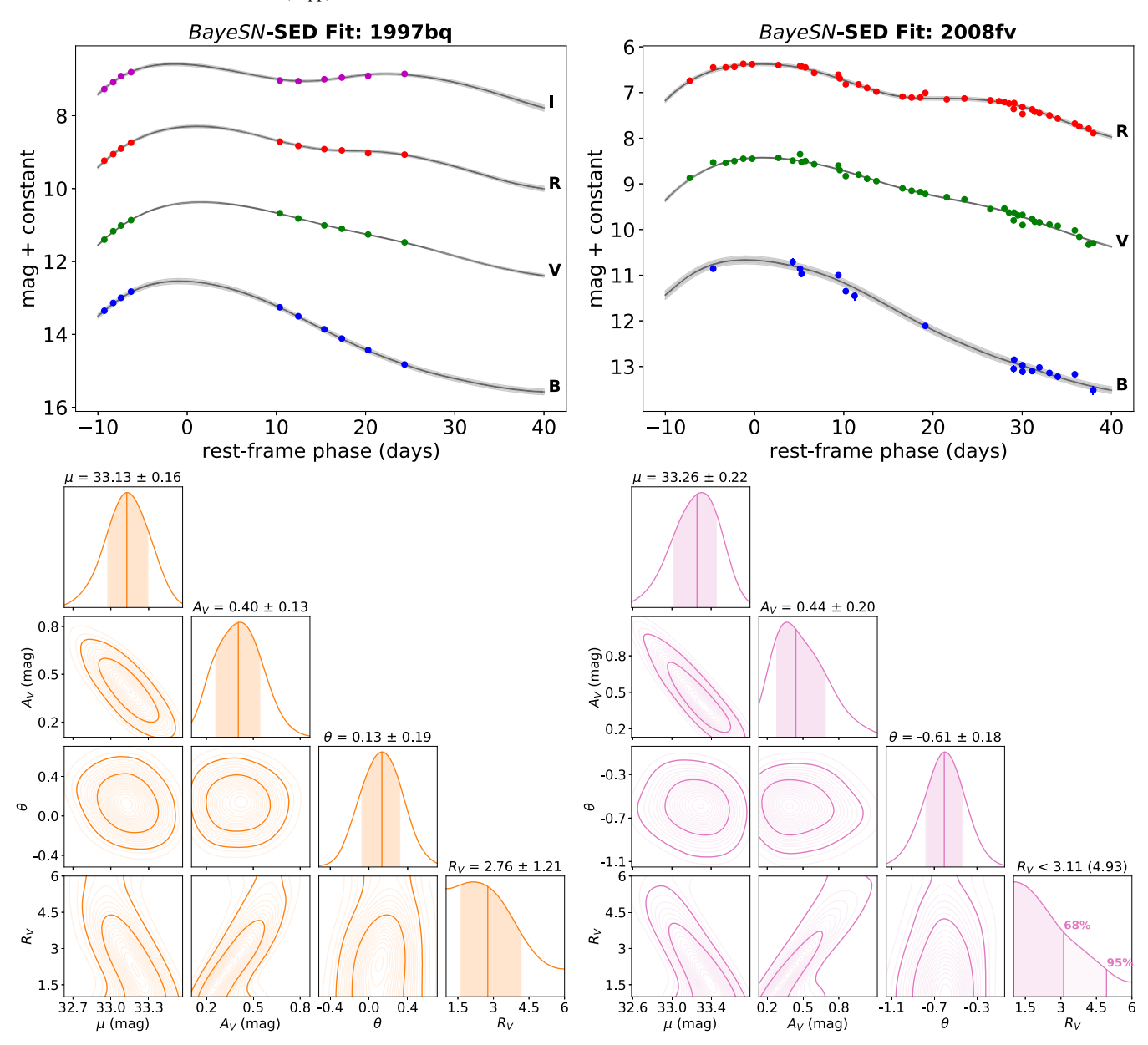


Figure 10. Individual BAYESN fits to SNe 1997bq and 2008fv (as in Figure 2). R_V posteriors are wide owing to the moderate extinction and lack of NIR data.

Table 5Posterior Summaries of SN Parameters from Individual Fits with $R_V^* = 2.659$ (i.e., R_V^s Fixed at the W22 Training Value)

Data Set	Bands	$\mu \text{ (mag)}$	A_V^s (mag)	θ_s	$\hat{\sigma}_{\mathrm{fit},s}(\mathrm{mag})^{\mathrm{a}}$
21hpr	grizy	33.142 ± 0.109	0.265 ± 0.043	-0.572 ± 0.096	0.053
97bq	BVRI	33.135 ± 0.115	0.402 ± 0.070	0.129 ± 0.191	0.065
08fv	BVR	33.224 ± 0.117	0.499 ± 0.074	-0.628 ± 0.167	0.070

Note.

Appendix C H_0 Methods & Additional Results

In the upper Hubble flow rung, we use distances to a high-stellar-mass subsample of 109 SNe Ia from the Foundation DR1 sample (Foley et al. 2018; Jones et al. 2019); this minimizes the systematic contribution from the mass step toward the H_0 inference (because NGC 3147 is also high-mass). We use W22 BAYESN $R_V^* = 2.659$ photometric distance

estimates, along with redshift-based distances obtained from estimates of cosmological redshift, and we adopt our fiducial cosmology from Riess et al. (2016): $(\Omega_M, \Omega_\Lambda, H_0) = (0.28, 0.72, 73.24 \, \mathrm{km \, s^{-1} \, Mpc^{-1}})$. We use redshifts from the NASA/IPAC Extragalactic Database (NED), corrected to the CMB frame using the flow model of Carrick et al. (2015).²² The

^a The fitting uncertainties, or "measurement errors," on the individual siblings distance estimates, computed using Equation (10).

https://cosmicflows.iap.fr/

Table 6Hubble Constant Constraints

SN Calibrator(s)	δM Modeling Assumption ^a	$H_0 ({\rm km s^{-1} Mpc^{-1}})$		
		$R_V^* = 2.659$ °	$R_V^s \sim \mathcal{U}(1, 6)$	
Individual Fit Distance b				
21hpr	_	77.9 ± 6.4	77.6 ± 6.6	
97bq	_	77.8 ± 6.6	77.4 ± 7.6	
08fv	_	80.9 ± 6.7	81.4 ± 8.7	
All Individual Fit Distances c				
(21hpr, 97bq, 08fv)	δM -Uncorrelated	78.7 ± 6.2	78.0 ± 6.4	
(21hpr, 97bq, 08fv)	δM -Mixed	78.6 ± 6.4	78.0 ± 6.5	
(21hpr, 97bq, 08fv)	δM -Common	78.8 ± 6.4	78.0 ± 6.5	
Siblings' Light Curves d				
(21hpr, 97bq, 08fv)	δM -Mixed	78.4 ± 6.1	$\textbf{78.4} \pm \textbf{6.5}^{\text{ f}}$	

Notes. Using the siblings trio, a Cepheid distance Riess et al. (2022), and a Hubble flow sample of 109 SNe Ia in high-stellar-mass host galaxies from foundation DR1 (Foley et al. 2018; Jones et al. 2019).

NGC 3147 Cepheid distance from Riess et al. (2022) comes from their "fit 1 Baseline" analysis that uses optical+NIR "reddening-free" Wesenheit magnitudes. We use the distance derived without the inclusion of any SNe Ia in any host (as in Table 6 in Riess et al. 2022). We add 0.025 mag in quadrature to the Cepheid distance uncertainty to account for the geometric distance error. The literature Cepheid distance is $\hat{\mu}_{NGC}^{Ceph}$ = 33.014 \pm 0.167 mag

 $\hat{\mu}_{\rm NGC\,3147}^{\rm Ceph}=33.014\pm0.167$ mag We sample a 5 $\log_{10}H_0$ parameter and transform the posterior samples to H_0 . We marginalize also over the SN Ia total intrinsic scatter, σ_0 , and the peculiar velocity dispersion, $\sigma_{\rm pec}$, which is primarily constrained by the set of Hubble flow BAYESN distance estimates and the redshift-based distances. The calibrator galaxy's true distance parameter, $\mu_{\rm NGC\,3147}$, has an uninformative prior. We also marginalize over ΔM_0 , which is the difference between the calibrated absolute magnitude constant of the SNe, and the fiducial value fixed during model training; without the calibrator galaxy, this parameter is degenerate with H_0 . Our priors are

$$\log_{10} H_0 \sim U(\log_{10} 50, \log_{10} 100)$$
 (C1)

$$\sigma_0 \sim U(0, 1) \tag{C2}$$

$$\sigma_{\rm pec}/c \sim U(0, 1)$$
 (C3)

$$\mu_{\text{NGC 3147}} \sim U(-\infty, +\infty)$$
 (C4)

$$\Delta M_0 \sim U(-2, 2). \tag{C5}$$

In Table 6, we show H_0 inferences are insensitive to various modeling assumptions in the calibrator galaxy. The default configuration is to simultaneously fit the siblings' *light curves* with the Cepheid and Hubble flow distances (see "Siblings'

Light Curves" block in Table 6). To demonstrate that these methodologies for siblings can be applied to distances obtained with any SN model, we perform additional H_0 inferences using only one of the individual siblings' distance estimates (Section 4.2; "Individual Fit Distance") or all individual siblings' distance estimates at the same time (Section 4.3; "All Individual Fit Distances"). These two-step inferences are faster to compute, so we test the sensitivity of H_0 estimates to the R_V^s assumptions, and the intrinsic scatter modeling assumptions, in the calibrator galaxy.

Appendix D Simulations

We present here two sets of simulations to show how the siblings' intrinsic scatter modeling assumptions affect the common distance uncertainties to a single siblings galaxy—and in turn the H_0 uncertainties in the distance ladder. We show that adopting the δM -Uncorrelated assumption returns underestimated distance uncertainties, and hence H_0 uncertainties, compared to those obtained when the true $\sigma_{\rm Rel}$ is known (provided the true $\sigma_{\rm Rel} < \sigma_0$).

First, we simulate three individual sibling distance estimates under a true distance $\mu=30$ mag, with individual fitting uncertainties $\hat{\sigma}_{\rm fit}=0.06$ mag (the median in the W22 sample), a total intrinsic scatter $\sigma_0=0.1$ mag, and various choices of relative intrinsic scatter: $\sigma_{\rm Rel}=(0,0.25,0.5,0.75,1)\times\sigma_0$. We then fit for the common distance, with $\sigma_0=0.1$ mag, and under the three intrinsic scatter modeling assumptions: δM -Uncorrelated ($\sigma_{\rm Rel}=\sigma_0$), δM -Mixed (where $\sigma_{\rm Rel}$ is marginalized over using a uniform prior $\sigma_{\rm Rel}\sim U(0,~\sigma_0)$), and δM -Common ($\sigma_{\rm Rel}=0$). We perform 100 simulations, then compare against δM -True inferences, when the true value of $\sigma_{\rm Rel}$ is known in each fit.

Table 7 shows the δM -Uncorrelated uncertainties are always smaller than the δM -True uncertainties when $\sigma_{Rel} < \sigma_0$. Therefore, adopting the δM -Uncorrelated assumption will always underestimate the common distance uncertainty, unless the siblings are in the extreme regime of being perfectly uncorrelated: $\sigma_{Rel} = \sigma_0$. The distance uncertainties increase as the siblings are assumed to be more correlated, and the most conservative estimates are obtained by adopting the δM -Common assumption (i.e., $\sigma_{Rel} = 0$). In the rows where $\sigma_{\rm Rel} \lesssim \sigma_0/2$, the δM -Mixed uncertainties are slightly underestimated, $\sim \mathcal{O}(1 \text{ mmag})$, compared to the δM -True uncertainties, which is reflective of the weak constraining power on σ_{Rel} in the small sample size limit. However, these underestimates are an order of magnitude smaller than the $\approx 0.02 - 0.04$ mag underestimates from adopting the δM -Uncorrelated assumption. The δM -Mixed uncertainties match or exceed the δM -True uncertainties for $\sigma_{\text{Rel}} \gtrsim \sigma_0/2$. Therefore, the most important modeling choice in the small sample size limit, which has the largest impact on sibling inferences, is whether to adopt the δM -Uncorrelated assumption or either of the δM -Mixed/ Common assumptions.

We further explore the effect of relative intrinsic scatter on inferences of H_0 , by assuming calibrator galaxies in the second rung of the distance ladder contain siblings. We simulate 40 calibrator galaxies with sibling pairs, and Cepheid distances with 0.1 mag measurement errors. In the third rung, we simulate 100 single-SN Hubble flow galaxies in the redshift range $z_{\rm CMB} \sim U(0.01, 0.1)$, with $\sigma_{\rm pec} = 150 \, {\rm km \, s^{-1} \, Mpc^{-1}}$, and heliocentric redshift measurement errors of 0.0005. The

^a Intrinsic scatter modeling assumptions in Table 3

b NGC 3147 is calibrated with an individual-fit distance estimate to one sibling.

^c NGC 3147 is calibrated using all three individual-fit distance estimates.

^d NGC 3147 is calibrated by jointly fitting the light curves of the sibling trio, while simultaneously fitting the Cepheid and Hubble flow distances.

^e Priors on R_V .

f Our best H_0 constraint.

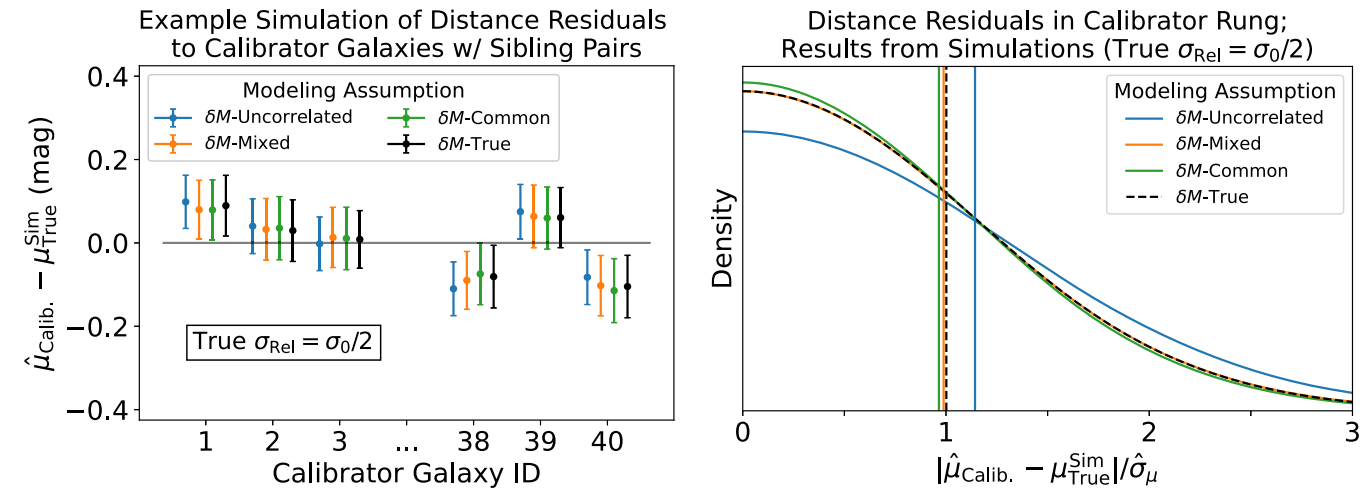


Figure 11. (Left panel) Example simulation showing the distance residuals to 40 calibrator galaxies with sibling pairs, where the true $\sigma_{\rm Rel} = \sigma_0/2 = 0.05$ mag. The distance residual, $\hat{\mu}_{\rm Calib.} - \mu_{\rm True}^{\rm Sim}$, compares the true distance in the simulation, $\mu_{\rm True}^{\rm Sim}$, with the calibrated SN siblings' common distance estimate to the calibrator galaxy, $\hat{\mu}_{\rm Calib.}$ (right panel) We plot a KDE of the 40 distance residuals, $|\hat{\mu}_{\rm Calib.} - \mu_{\rm True}^{\rm Sim}|/\hat{\sigma}_{\mu}$, averaged over 100 simulations, which shows how well-estimated the calibrator galaxy distance uncertainties are. For each galaxy, we take the posterior median distance estimate and divide by the posterior standard deviation, $\hat{\sigma}_{\mu}$; the vertical lines show the 68% quantiles, which should be close to unity if the uncertainties are well estimated. The uncertainties are overestimated when adopting the δM -Common assumption (where $\sigma_{\rm Rel} = 0$ is assumed), whereas the δM -Uncorrelated uncertainties are underestimated (where $\sigma_{\rm Rel} = \sigma_0$ is assumed). The δM -Mixed results (where $\sigma_{\rm Rel}$ is marginalized over) and the δM -True results (where $\sigma_{\rm Rel}$ is known and fixed in the model fit) agree with one another; moreover, the 68% quantiles are strongly consistent with unity, indicating the distance uncertainties are well-calibrated.

 Table 7

 Common Distance Uncertainties from Three Simulated Siblings' Distances, Averaged across 100 Simulations

# Siblings	True σ_{Rel}	$\hat{\sigma}_{\!\mu} \; ({ m mag})^{ m a}$					
// 2.5gs	- Rei	δM -Uncorrelated	δM -Mixed	δM-Common	δM-True ^b		
3	0	0.067 ± 0.001	0.097 ± 0.002	0.106 ± 0.001	0.106 ± 0.001		
3	$\sigma_0/4$	0.067 ± 0.001	0.097 ± 0.003	0.105 ± 0.001	0.104 ± 0.001		
3	$\sigma_0/2$	0.067 ± 0.001	0.096 ± 0.004	0.106 ± 0.001	0.098 ± 0.001		
3	$3\sigma_0/4$	0.067 ± 0.001	0.095 ± 0.005	0.106 ± 0.001	0.086 ± 0.001		
3	σ_0	0.067 ± 0.001	0.092 ± 0.006	0.106 ± 0.001	0.067 ± 0.001		

Notes.

^a The median and sample standard deviation of common distance uncertainties across 100 simulations (details in text).

^b Uncertainty on the common- μ inference when the true $\sigma_{\rm Rel}$ is known and fixed in the model.

Table 8 H_0 Recovery across 100 Simulations, Where Siblings Calibrator Galaxies Each Have a Sibling Pair, and $\sigma_0 = 0.1$ mag

# Siblings	# Calibrators	True σ_{Rel}	$\hat{\sigma}_{Rel} (mag)^a$		$\hat{\sigma}_{H_0}$ (km s ⁻¹	1 Mpc ⁻¹)	
Calibrators	"	T.C.	δM -Mixed	δM -Uncorrelated	δM -Mixed	δM -Common	δM-True b
40	40	0	< 0.03(0.05)	0.77 ± 0.01	0.85 ± 0.01	0.85 ± 0.01	0.85 ± 0.01
40	40	$\sigma_0/4$	0.03 ± 0.02	0.77 ± 0.01	0.85 ± 0.01	0.85 ± 0.01	0.85 ± 0.01
40	40	$\sigma_0/2$	0.05 ± 0.02	0.77 ± 0.01	0.83 ± 0.01	0.85 ± 0.01	0.83 ± 0.01
40	40	$3\sigma_0/4$	0.07 ± 0.02	0.77 ± 0.01	0.80 ± 0.02	0.85 ± 0.01	0.81 ± 0.01
40	40	σ_0	>0.08(0.06)	0.77 ± 0.01	0.79 ± 0.01	0.85 ± 0.01	0.77 ± 0.01

Notes.

^a The σ_{Rel} posterior summary from the δM -Mixed fit simulations. For the posteriors peaking at the lower or upper prior boundaries, the 68% and 95% quantiles, or the 32% and 5% quantiles, are quoted, respectively.

^b H_0 Inference when σ_{Rel} is known and fixed in the model.

simulated true Hubble constant is $H_0 = 70 \, \mathrm{km \, s^{-1} \, Mpc^{-1}}$. As above, we assess recovery of H_0 for different intrinsic scatter modeling assumptions. Table 8 shows the H_0 uncertainties are underestimated with the δM -Uncorrelated assumption, in all cases except for when the true $\sigma_{\mathrm{Rel}} = \sigma_0$. With 40 sibling pairs, σ_{Rel} is constrained well, to the extent that the δM -Mixed

uncertainties agree strongly with the δM -True uncertainties for all $\sigma_{\rm Rel}$ values.

To better intuit these simulations, we plot the distance residuals and their uncertainties in Figure 11. The left panel shows an example simulation, where the true $\sigma_{\text{Rel}} = \sigma_0/2$. The right panel shows a KDE of the 40 distance residuals,

normalized by their uncertainties, averaged over 100 simulations. With well-calibrated uncertainties, the distance residuals should be $\approx\!1\sigma$ consistent with zero in 68% of simulations; however, the residuals are consistent with zero in less than 68% of simulations if the uncertainties are underestimated, and vice versa. The right panel shows the δM -Common, -Mixed, and -Uncorrelated assumptions lead to overestimated, well-calibrated, and underestimated uncertainties, respectively.

ORCID iDs

Sam M. Ward https://orcid.org/0000-0002-1763-2720 Kaisey S. Mandel https://orcid.org/0000-0001-9846-4417 Suhail Dhawan https://orcid.org/0000-0002-2376-6979 David O. Jones https://orcid.org/0000-0002-6230-0151 Ryan J. Foley https://orcid.org/0000-0002-2445-5275 Gautham Narayan https://orcid.org/0000-0001-6022-0484 Kenneth C. Chambers https://orcid.org/0000-0001-6965-7789 David A. Coulter https://orcid.org/0000-0003-4263-2228 Kyle W. Davis https://orcid.org/0000-0002-5680-4660 Thomas de Boer https://orcid.org/0000-0001-5486-2747 Alex Gagliano https://orcid.org/0000-0003-4906-8447 Hua Gao https://orcid.org/0000-0003-1015-5367 Jens Hjorth https://orcid.org/0000-0002-4571-2306 Mark E. Huber https://orcid.org/0000-0003-1059-9603 Luca Izzo https://orcid.org/0000-0001-9695-8472 Danial Langeroodi https://orcid.org/0000-0001-5710-8395 Eugene A. Magnier https://orcid.org/0000-0002-7965-2815 Armin Rest https://orcid.org/0000-0002-4410-5387 César Rojas-Bravo https://orcid.org/0000-0002-7559-315X

References

```
Abbott, T. M. C., Allam, S., Andersen, P., et al. 2019, ApJL, 872, L30
Avelino, A., Friedman, A. S., Mandel, K. S., et al. 2019, ApJ, 887, 106
Barna, B., Nagy, A. P., Bora, Zs., et al. 2023, A&A, 677, A183
Bishop, C. M. 2006, Pattern Recognition and Machine Learning (Berlin:
Biswas, R., Goobar, A., Dhawan, S., et al. 2022, MNRAS, 509, 5340
Briday, M., Rigault, M., Graziani, R., et al. 2022, A&A, 657, A22
Brout, D., & Scolnic, D. 2021, ApJ, 909, 26
Brout, D., Scolnic, D., Popovic, B., et al. 2022, ApJ, 938, 110
Brown, P. J., Smitka, M. T., Wang, L., et al. 2015, ApJ, 805, 74
Burns, C. R., Ashall, C., Contreras, C., et al. 2020, ApJ, 895, 118
Burns, C. R., Stritzinger, M., Phillips, M. M., et al. 2011, AJ, 141, 19
Carpenter, B., Gelman, A., Hoffman, M. D., et al. 2017, J. Stat. Software, 76, 1
Carrick, J., Turnbull, S. J., Lavaux, G., & Hudson, M. J. 2015, MNRAS,
Chambers, K. C., Magnier, E. A., Metcalfe, N., et al. 2016, arXiv:1612.05560
Childress, M., Aldering, G., Antilogus, P., et al. 2013, ApJ, 770, 108
Coe, D., Umetsu, K., Zitrin, A., et al. 2012, ApJ, 757, 22
Coulter, D. A., Jones, D. O., McGill, P., et al. 2022, YSE-PZ: An Open-source
   Target and Observation Management System, v0.3.0, Zenodo, doi:10.5281/
   zenodo.7278430
Coulter, D. A., Jones, D. O., McGill, P., et al. 2023, PASP, 135, 064501
D'Andrea, C. B., Gupta, R. R., Sako, M., et al. 2011, ApJ, 743, 172
Dhawan, S., Goobar, A., Smith, M., et al. 2022, MNRAS, 510, 2228
Dhawan, S., Thorp, S., Mandel, K. S., et al. 2023, MNRAS, 524, 235
Dimitriadis, G., Foley, R. J., Arendse, N., et al. 2022, ApJ, 927, 78
Draine, B. 2003, ARA&A, 41, 241
Elias, J. H., Frogel, J. A., Hackwell, J. A., & Persson, S. E. 1981, ApJL,
   251, L13
Fitzpatrick, E. L. 1999, PASP, 111, 63
Foley, R. J., Scolnic, D., Rest, A., et al. 2018, MNRAS, 475, 193
Freedman, W. L. 2021, ApJ, 919, 16
Friedman, A. S., Wood-Vasey, W. M., Marion, G. H., et al. 2015, ApJS, 220, 9
Gagliano, A., Izzo, L., Kilpatrick, C. D., et al. 2022, ApJ, 924, 55
Gall, C., Stritzinger, M. D., Ashall, C., et al. 2018, A&A, 611, A58
Gallego-Cano, E., Izzo, L., Dominguez-Tagle, C., et al. 2022, A&A, 666, A13
```

```
Gelman, A., Carlin, J. B., Stern, H. S., et al. 2013, Bayesian Data Analysis (3rd
  edn.; New York: Chapman & Hall/CRC)
Graham, M. L., Fremling, C., Perley, D. A., et al. 2022, MNRAS, 511, 241
Guy, J., Astier, P., Baumont, S., et al. 2007, A&A, 466, 11
Guy, J., Sullivan, M., Conley, A., et al. 2010, A&A, 523, A7
Hamuy, M., Phillips, M. M., Maza, J., et al. 1991, AJ, 102, 208
Hicken, M., Challis, P., Jha, S., et al. 2009, ApJ, 700, 331
Hicken, M., Challis, P., Kirshner, R. P., et al. 2012, ApJS, 200, 12
Hoogendam, W. B., Ashall, C., Galbany, L., et al. 2022, ApJ, 928, 103
Hounsell, R., Scolnic, D., Foley, R. J., et al. 2018, ApJ, 867, 23
Itagaki, K. 2021, TNSR, 2021-998, 1
Jacobson-Galán, W. V., Venkatraman, P., Margutti, R., et al. 2022a, ApJ,
Jacobson-Galán, W. V., Dessart, L., Jones, D. O., et al. 2022b, ApJ, 924, 15
Jha, S., Garnavich, P., Challis, P., et al. 1999, IAU Circ., 7206, 1
Jha, S., Kirshner, R. P., Challis, P., et al. 2006, AJ, 131, 527
Johansson, J., Cenko, S. B., Fox, O. D., et al. 2021, ApJ, 923, 237
Jones, D. O., Foley, R. J., Narayan, G., et al. 2021, ApJ, 908, 143
Jones, D. O., Mandel, K. S., Kirshner, R. P., et al. 2022, ApJ, 933, 172
Jones, D. O., Riess, A. G., Scolnic, D. M., et al. 2018, ApJ, 867, 108
Jones, D. O., Scolnic, D. M., Foley, R. J., et al. 2019, ApJ, 881, 19
Ivezić, Ž., Kahn, S. M., Tyson, J. A., et al. 2019, ApJ, 873, 111
Kelly, P. L., Hicken, M., Burke, D. L., Mandel, K. S., & Kirshner, R. P. 2010,
Kelsey, L. 2023, arXiv:2303.02020
Kelsey, L., Sullivan, M., Smith, M., et al. 2021, MNRAS, 501, 4861
Kilpatrick, C. D., Drout, M. R., Auchettl, K., et al. 2021, MNRAS, 504,
Krisciunas, K., Contreras, C., Burns, C. R., et al. 2017, AJ, 154, 211
Krisciunas, K., Garnavich, P. M., Stanishev, V., et al. 2007, AJ, 133, 58
Krisciunas, K., Phillips, M. M., Suntzeff, N. B., et al. 2004a, AJ, 127, 1664
Krisciunas, K., Suntzeff, N. B., Candia, P., et al. 2003, AJ, 125, 166
Krisciunas, K., Suntzeff, N. B., Phillips, M. M., et al. 2004b, AJ, 128, 3034
Leloudas, G., Stritzinger, M. D., Sollerman, J., et al. 2009, A&A, 505, 265
Lim, G., Im, M., Paek, G. S. H., et al. 2023, ApJ, 949, 33
Mandel, K. S., Thorp, S., Narayan, G., Friedman, A. S., & Avelino, A. 2022,
        RAS, 510, 3939
Meldorf, C., Palmese, A., Brout, D., et al. 2023, MNRAS, 518, 1985
Miller, J. S., & Stone, R. P. S. 1993, Lick Observatory, Tech. Rep. 66, Lick
  Observatory
Pan, Y.-C., Sullivan, M., Maguire, K., et al. 2014, MNRAS, 438, 1391
Perlmutter, S., Aldering, G., Goldhaber, G., et al. 1999, ApJ, 517, 565
Phillips, M. M. 1993, ApJL, 413, L105
Pignata, G., Benetti, S., Mazzali, P. A., et al. 2008, MNRAS, 388, 971
Planck Collaboration, Aghanim, N., Akrami, Y., et al. 2020, A&A, 641, A6
Ponder, K. A., Wood-Vasey, W. M., Weyant, A., et al. 2021, ApJ, 923, 197
Popovic, B., Brout, D., Kessler, R., & Scolnic, D. 2021, arXiv:2112.04456
Rahman, N., Bolatto, A. D., Xue, R., et al. 2012, ApJ, 745, 183
Rest, A., Stubbs, C., Becker, A. C., et al. 2005, ApJ, 634, 1103
Riess, A. G., Filippenko, A. V., Challis, P., et al. 1998, AJ, 116, 1009
Riess, A. G., Kirshner, R. P., Schmidt, B. P., et al. 1999, AJ, 117, 707
Riess, A. G., Macri, L. M., Hoffmann, S. L., et al. 2016, ApJ, 826, 56
Riess, A. G., Yuan, W., Macri, L. M., et al. 2022, ApJL, 934, L7
Rigault, M., Brinnel, V., Aldering, G., et al. 2020, A&A, 644, A176
Rigault, M., Copin, Y., Aldering, G., et al. 2013, A&A, 560, A66
Roman, M., Hardin, D., Betoule, M., et al. 2018, A&A, 615, A68
Rose, B. M., Baltay, C., Hounsell, R., et al. 2021, arXiv:2111.03081
Rose, B. M., Rubin, D., Cikota, A., et al. 2020, ApJL, 896, L4
Schlafly, E. F., Meisner, A. M., Stutz, A. M., et al. 2016, ApJ, 821, 78
Scolnic, D., Brout, D., Carr, A., et al. 2022, ApJ, 938, 113
Scolnic, D., Perlmutter, S., Aldering, G., et al. 2019, Astro2020: Decadal
  Survey on Astronomy and Astrophysics, science white papers 270,
Scolnic, D., Smith, M., Massiah, A., et al. 2020, ApJL, 896, L13
Silverman, J. M., Foley, R. J., Filippenko, A. V., et al. 2012, MNRAS,
  425, 1789
Smith, M., Sullivan, M., Wiseman, P., et al. 2020, MNRAS, 494, 4426
Sorai, K., Kuno, N., Muraoka, K., et al. 2019, PASJ, 71, S14
Stahl, B. E., de Jaeger, T., Boruah, S. S., et al. 2021, MNRAS, 505, 2349
Stan Development Team 2020, Stan Modelling Language Users Guide and
  Reference Manual v.2.25, https://mc-stan.org
Stanishev, V., Goobar, A., Benetti, S., et al. 2007, A&A, 469, 645
Stritzinger, M. D., Phillips, M. M., Boldt, L. N., et al. 2011, AJ, 142, 156
Sullivan, M., Conley, A., Howell, D. A., et al. 2010, MNRAS, 406, 782
Sullivan, M., Ellis, R. S., Aldering, G., et al. 2003, MNRAS, 340, 1057
Terreran, G., Jacobson-Galán, W. V., Groh, J. H., et al. 2022, ApJ, 926, 20
The LSST Dark Energy Science Collaboration, Mandelbaum, R., Eifler, T.,
  et al. 2018, arXiv:1809.01669
```

Thorp, S., & Mandel, K. S. 2022, MNRAS, 517, 2360Thorp, S., Mandel, K. S., Jones, D. O., Ward, S. M., & Narayan, G. 2021, MNRAS, 508, 4310

Tinyanont, S., Ridden-Harper, R., Foley, R. J., et al. 2022, MNRAS, 512, 2777 Tsvetkov, D. Y., & Elenin, L. 2010, PZ, 30, 2

Uddin, S. A., Burns, C. R., Phillips, M. M., et al. 2020, ApJ, 901, 143

Uddin, S. A., Mould, J., Lidman, C., Ruhlmann-Kleider, V., & Zhang, B. R. 2017, ApJ, 848, 56

Wiseman, P., Vincenzi, M., Sullivan, M., et al. 2022, MNRAS, 515, 4587 Wood-Vasey, W. M., Friedman, A. S., Bloom, J. S., et al. 2008, ApJ, 689, 377 Yim, K., & van der Hulst, J. M. 2016, MNRAS, 463, 2092

Zhang, Y., Zhang, T., Danzengluobu, et al. 2022, PASP, 134, 074201